Title

The nematode worm *C. elegans* chooses between bacterial foods exactly as if maximizing economic utility

Authors

Abraham Katzen[1], Hui-Kuan Chung[2,3]*, William T. Harbaugh[4]*, Christina Della Iacono[1], Nicholas Jackson[1], Stephanie K. Yu[4], Steven W. Flavell[4], Paul W. Glimcher[2,3], Shawn R. Lockery[1]

1. Institute of Neuroscience, University of Oregon, Eugene OR, USA

2. Center for Neural Science, New York University, New York, NY, USA

3. Neuroscience Institute, New York University School of Medicine, New York, NY, USA.

4. Department of Economics, University of Oregon, Eugene OR, USA

5. Picower Institute for Learning and Memory, Department of Brain & Cognitive Sciences, Massachusetts Institute of Technology, Cambridge, MA, USA

* Equal contribution

Abstract

In value-based decision making, options are selected according to subjective values assigned by the individual to available goods and actions. Despite the importance of this faculty of the mind, the neural mechanisms of value assignments, and how choices are directed by them, remain obscure. To investigate this problem, we used a classic measure of utility maximization, the Generalized Axiom of Revealed Preference, to quantify internal consistency of food preferences in *Caenorhabditis elegans*, a nematode worm with a nervous system of only 302 neurons. Using a novel combination of microfluidics and electrophysiology, we found that *C. elegans* food choices fulfill the necessary and sufficient conditions for utility maximization, indicating that nematodes behave exactly as if they maintain, and attempt to maximize, an underlying representation of subjective value. Food choices are well-fit by a utility function widely used to model human consumers. Moreover, as in many other animals, subjective values in *C. elegans* are learned, a process we now find requires intact dopamine signaling. Differential responses of identified chemosensory neurons to foods with distinct growth potential are amplified by prior consumption of these foods, suggesting that these neurons may be part of a value-assignment system. The demonstration of utility maximization in an organism with a nervous system of only 302 neurons sets a new lower bound on the computational requirements for its execution, and offers the prospect of an essentially complete explanation of value-based decision making at single neuron resolution.

Introduction

One of the primary functions of the human brain is to make decisions that maximize individual *welfare*. Welfare is fundamentally subjective, based on values the individual assigns idiosyncratically, and privately, to goods and outcomes. Can welfare maximization nevertheless be investigated in objective terms? One solution to this problem is revealed preference theory (Samuelson, 1938) which identifies the patterns of behavior, observable as such, that are necessary and sufficient evidence that subjects are choosing in ways consistent with welfare maximization or, in economic terminology, *utility maximization*. These patterns have been defined mathematically by the Generalized Axiom of Revealed Preference (GARP) (Houthakker, 1950; Afriat, 1967; Varian, 1982). A growing number of studies have utilized GARP to quantify utility maximization in children and adults under a variety of economic and physiological conditions (Harbaugh, Krause and Berry, 2001; Andreoni and Miller, 2002; Burghart, Glimcher and Lazzaro, 2013; Lazzaro *et al.*, 2016).

GARP is significant for the neuroscience of decision making because it provides a definitive behavioral test for utility maximization, or its absence. This test can be applied in to almost any organism that makes

choices between desirable goods that incur costs. The basic concept underlying this axiom is that a maximizing agent's choices must be internally consistent. If the agent is observed to prefer X over Y when both are available then, other things being equal, the agent should not also prefer Y over X, a pattern that is obviously inconsistent. Importantly, internal consistency must extend to preferences revealed indirectly, through transitivity. For example, an individual observed to choose X over Y and Y over Z, has indirectly revealed that they should choose X over Z. If instead Z is chosen over X, then their decision making cannot be an instance of goal-directed maximization in any significant sense of the term.

The number and severity of GARP violations (assuming the agent is motivated to maintain or improve its welfare), has been taken as a measure of cognitive function (Camille *et al.*, 2011). It can also be correlated with physical variables such as neuroanatomy and neuronal activity (Chung, Tymula and Glimcher, 2017; Pastor-Bernier, Stasiak and Schultz, 2019). These studies reveal the range of insights that can be gained by combining revealed preference theory and neuroscience.

To our knowledge, however, tests for utility maximization using GARP have yet to be applied to organisms more amenable to mechanistic studies such as mice, zebrafish, fruit flies, and nematodes. A major goal of this study was to determine whether food choices of the nematode *C. elegans*, a microscopic round worm with a nervous system of only 302 neurons, are consistent with GARP and thus exhibit a form of utility maximization. A positive result would establish a simple experimental system in which neuronal activity correlated with utility could be manipulated both physiologically and genetically to establish behavioral causality. Such a finding would also be interesting from a comparative perspective, extending the domain of utility-based decision making far beyond the boundaries of organisms that are generally considered to have cognition.

A microscopic worm might seem a surprising choice for investigating utility maximization. However, *C. elegans* possesses a sophisticated behavioral repertoire that can be organized into to three broad functional categories (Faumont, Lindsay and Lockery, 2012; Yapici, Zimmer and Domingos, 2014): (1) maintenance behaviors, such as feeding, defecation, mating, and egg laying; (2) escape reflexes, for avoiding life threatening conditions such as noxious heat, ultraviolet light, high oxygen or CO_2, toxins, desiccation, and predation by fungi, mites, and other nematodes; and (3) habitat and resource-localization behaviors, including a variety of spatial orientation strategies that enable *C. elegans* to obtain goods such as hospitable living conditions and resources (e.g., food and mating partners), and to avoid inhospitable conditions and the lack of resources.

C. elegans exhibits a considerable range of decision making behaviors (Faumont, Lindsay and Lockery, 2012; Yapici, Zimmer and Domingos, 2014): (1) action versus inaction, such as probabilistic withdrawal responses(Culotti and Russell, 1978; Chalfie *et al.*, 1985; Shinkai, Yamamoto, Fujiwara, Tabata, Murayama, Hirotsu, Daisuke D. Ikeda, *et al.*, 2011); (2) approach versus avoidance, such as when an initially attractive odor or taste is made aversive by pairing it with the absence of food (Colbert and Bargmann, 1995; Saeki, Yamamoto and Iino, 2001; Torayama, Ishihara and Katsura, 2007); (3) appetitive choice, such as when worms are presented with a choice between benign or pathogenic food (Zhang, Lu and Bargmann, 2005); and (4) choice under risk, such as when worms must decide whether to risk crossing a potentially lethal chemical barrier to obtain food (Shinkai, Yamamoto, Fujiwara, Tabata, Murayama, Hirotsu, Daisuke D Ikeda, *et al.*, 2011). Other examples include the choice to remain in a food patch rather than to leave to find a mate (Barrios, Nurrish and Emmons, 2008) or the choice to remain in a dwindling patch of food rather than leave for a possibly better patch (Bendesky *et al.*, 2011; Milward *et al.*, 2011); the latter has strong parallels with optimal foraging theory (Busch and Olofsson, 2012). *C. elegans* has also been shown to exhibit bounded rationality (Simon, 1957), a property it shares with humans and most other animals. Its pairwise preferences for attractive odors generally obey transitivity but with a considerable number of exceptions (Iwanir *et al.*, 2019). Similarly, its pairwise preferences are not generally influenced by introduction of a third option in the choice set, another classical mark of rationality, but again with a considerable number of exceptions (Cohen *et al.*, 2019). However, none of these preference tests provide necessary and sufficient evidence for utility maximization.

We selected food choice as the behavior most favorable for studies of utility maximization in a worm. *C. elegans* is an omnivorous bacterivore that mainly inhabits rotting plant material such as decaying fruits and

fleshy stems (Frezal and Felix, 2015). Its natural habitat contains thousands of different species of bacteria (Samuel *et al.*, 2016), including many beneficial and pathogenic varieties. Each beneficial species has a characteristic nutritional quality defined in terms of the growth rate of individual worms cultured on that species (Avery and Shtonda, 2003; Samuel *et al.*, 2016). In contrast, pathogenic species can be lethal (Tan *et al.*, 1999). Thus food choice has immediate fitness consequences for the worm, and it is reasonable to expect that *C. elegans* food choices maximize fitness. Fitness is basically an objective measure of welfare. In simple organisms with a limited repertoire of motivations, there is ought to be few opportunities for subjective and objective measures of welfare to diverge. This observation offers some confidence that the worm should maximize utility, or nearly so (Kacelnik, 2006).

C. elegans larvae hatch with little or no knowledge of the nutritional quality of bacteria (Shtonda and Avery, 2006). Instead, worms learn which bacteria species are better to eat by sampling what is available. For example, hatchlings are equally attracted to lawns of high and medium quality bacteria but after being allowed to sample both for several hours, they acquire robust preference for high quality bacteria (Shtonda and Avery, 2006). Additionally, adult worms will feed more readily on beneficial bacteria remembered from previous encounters than on novel beneficial bacteria, a form of latent learning referred to as the familiar food effect (Song *et al.*, 2013). In another example, the preference of naive adults for pathogenic bacteria is reversed after they sample and consume them (Zhang, Lu and Bargmann, 2005). Worms can also develop preferences over beneficial bacteria having different levels of nutritional quality. The establishment of preferences through sampling suggests an association is formed between the particular mixtures of odors present in particular foods and relative nutritional gain, a form of classical conditioning we refer to as *explicit food quality learning*.

In this study we utilized GARP to test for utility maximization and investigated its behavioral and neuronal mechanisms. This was accomplished by means of a microfluidic device that enabled us to offer single, semi-restrained worms high and medium quality bacteria at a range of different relative abundances while monitoring consumption electrophysiologically. We found that *C. elegans* food choices in naïve and trained animals are consistent with utility maximization. Worms behave as if they employed an underlying representation of utility which they were acting to maximize. Preference data were well fit by a utility function widely used to model the behavior of human consumers. At the behavioral level, utility maximization relies on a chemotaxis strategy known as *klinotaxis*. In this strategy, head bends during sinusoidal during locomotion are biased by chemosensory input such that bend are deeper on this side where attractant concentration is greater. At the neuronal level, we found that chemosensory neurons known to modulate head position are able to discriminate between high and medium quality food, and that food quality training increases this ability. These findings establish a new model system in which to investigate the neuronal and genetic basis of subjective value (the neural correlate of utility), and its behavioral expression

Results

GARP for worms

In a GARP experiment for human subjects (Harbaugh, Krause and Berry, 2001), each person is given a series of *choice sets*. A choice set comprises a list of options, called *bundles*, from which the person is asked to pick the bundle they most prefer. Choices sets are constructed so that selections are made from varying quantities of a pair of goods (e.g., apples and oranges; Fig. 1A). Each choice set is defined by a unique combination of prices and budget. As each bundle consumes the entire budget (in units of money or time), a bundle with more of one good has less of the other, yielding an inherent tradeoff between goods.

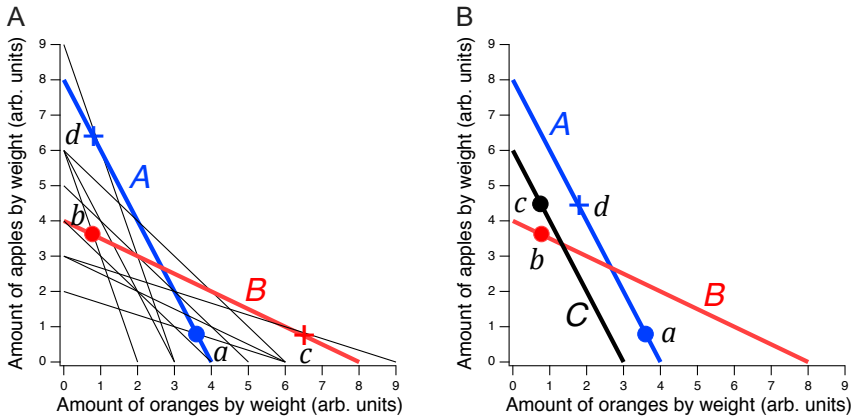

Figure 1. Design of a GARP experiment and tests for utility maximization

A. Experimental design and illustration of a direct violation of utility maximization. Diagonal lines indicate choice sets (n = 11). Choice sets are distinguished by having different values of the overall budget (which must be spent completely) and/or different prices for at least one of the goods. To choice sets are highlighted by color. *A*: budget is \$8, oranges are \$2 per unit, apples are \$1 per unit; *B*: budget = \$8, oranges are \$1 per unit, apples are \$2 per unit. *Filled circles*, chosen amounts; *plus signs*, available amounts not chosen. Given the choices shown and the more is better rule, $a \succcurlyeq d \succ b \Longrightarrow a \succ b$ and $b \succcurlyeq c \succ a \Longrightarrow b \succ a$. The choices a and b directly violate utility maximization. **B**. Indirect violation of utility maximization. Symbols as in A. The choices a and c constitute an indirect violation of utility maximization as described in the text.

Fig. 1A shows an ensemble of such choice sets, each of which can be conceptualized as offering the two goods at different prices. The lines in the figure, called *budget lines*, depict the pricing constraints and trade-offs particular to each choice set. In *A*, for example, the person must forgo two units of oranges for each additional unit of apples; in economic parlance, oranges in *A* are half the "price" of apples. Choosing is construed as selecting the most preferred option from those available in the choice set. The constellation of choices a person makes across the many different choice sets in the ensemble is analyzed for the presence of combinations that cannot possibly be consistent with utility maximization. We refer to these as *violations* of utility maximization. The consistent absence of violations, in an ensemble containing numerous choices that would violate consistency, is taken as evidence for of utility maximization. Here we provide a non-technical explanation of the underlying theory; technical treatments are available elsewhere (Varian, 1982; Harbaugh, Krause and Berry, 2001; Burghart, Glimcher and Lazzaro, 2013).

Utility violations can be direct or indirect. In the test we employ, both types of violation depend on the assumption that more of a good is better than less of it (strong monotonicity of utility). The filled circles in Fig. 1A are one possible pair of choices, a and b, selected to exemplify a *direct* violation. In choice set *A*, a was selected over d, which was also in the choice set but was not chosen. We infer from this choice that a is at least as good as d, which we write as $a \succcurlyeq d$. (We cannot conclude that a is better than d because the person could have been indifferent between them, with a being chosen randomly.) Noting that d has the same number of oranges but more apples than b, we infer by strong monotonicity that d is *strictly* preferred to b, written as $d \succ b$. Combining the inferences $a \succcurlyeq d$ and $d \succ b$, we conclude that a should be strictly preferred to b, that is, it should also be true that $a \succ b$. This preference is said to be revealed *directly*, because when people choose a, they do so over another option on the same budget line, d, that has more of at least one of the goods than b. Similar logic applies to choice set *B* such that b is directly revealed preferred to a, that is, $b \succ a$. These two preferences constitute a violation because they are inconsistent; there is no underlying maximization process of any kind that could allow for this combination of preferences.

A person *indirectly* reveals a preference for one bundle over another when there is a *sequence* of directly revealed preferences that link the two by transitivity. Fig. 1B illustrates an indirect violation of utility maximization. In addition to the original choices a and b, the person picked c in choice set *C*. We observe that c is directly revealed preferred to b because it has more of at least one good than the latter, so $c \succ b$. And, as before, $b \succ a$, from which we conclude by transitivity that c is preferred to a. We write this as $c \succ\!* a$, where the asterisk indicates indirectness. However, at the same time the person reveals $a \succcurlyeq d$ while $d \succ c$, from which we conclude $a \succ c$. These two preferences constitute a violation because they are inconsistent; again, no maximization process could allow for this combination of preferences. Further, it can be shown that when only two goods are available, the presence of direct violations is a necessary condition for indirect violations (Rose, 1958; Heufer, 2009). This fact is the foundation for the neuronal mechanism of utility maximization proposed in the Discussion.

Establishment of prerequisites for GARP experiments in *C. elegans*

The foregoing examples illustrate that a GARP experiment entails the following prerequisites: (i) goods that agents would like to consume, and the more the better; (ii) observations of the agent's choices of consumption of each good at under various budget and price constraints, and (iii) decisions on intersecting choice sets. The first step in this study was to develop and validate the means to fulfill these prerequisites in ecologically realistic ways for *C. elegans*.

Prerequisite (i): goods. To represent the two goods in a GARP experiment, we used bacteria species having high (H) and medium (M) quality as a food source, *Comamonus* and *Bacillus simplex*, respectively (Avery and Shtonda, 2003; Shtonda and Avery, 2006). We chose to work with adults worms as they are easier to handle and count than the L1 larvae used in previous food-choice experiments. It was initially unknown whether older worms could learn new palatable food preferences, so we began by investigating the magnitude, neuronal dependence, and mechanisms of explicit food quality learning in the developmental period spanning late L3 to young adulthood.

Synchronized, late L3 worms (N2) were transferred to a training plate which contained an equal number of similar sized patches of H and M foods (Fig. 2A, Trained). Preference for H versus M food was assessed

the following day at the young adult stage on a test plate having a single pair of H and M food patches (henceforth, the "open-field accumulation assay"). Control worms were transferred to a mock training plate and tested in parallel with trained worms (Fig. 2A, Untrained). Preference index I was quantified on a scale such that +1 and -1 represent absolute preference for H and M food, respectively; 0 represents indifference. Note that accumulation assays are not the same as the revealed preference assays used later in this study to investigate utility maximization. In particular, accumulation assays do not allow worms to consume mixtures of the goods (bundles) in the same feeding bout, nor do they challenge worms with different relative food densities (prices).

Trained N2 worms preferred H food to M food more strongly than untrained worms (Fig. 2B, N2, Trained vs. Untrained, Supplemental Table 1[1]) indicating a significant effect of food quality training. We conclude that worms in the developmental period under study can learn new food preferences. However, untrained N2 worms also preferred H to M food even though they were encountering these foods for the first time (Fig. 2B, N2 Untrained, $I > 0$, Supplemental Table 1[2]). Thus, either developmental time or exposure of untrained animals to *E. coli* during the growth and/or training phase of the experiment somehow induces a latent preference for H over and M food at first encounter. If H food smells to the worm more like *E. coli* than M food does, this preference might be explained by the so-called food familiarity effect (Song *et al.*, 2013), in which worms eat familiar food more readily than novel food.

C. elegans has 11 pairs of anterior chemosensory neurons that respond to bacteria conditioned medium (Zaslaver *et al.*, 2015), acting either as on-cells (activated by onset), or off-cells (activated by offset). As a first step in identifying the locus of explicit food quality learning, we measured food preferences in worms with loss of function mutation in the *ceh-36* Otx homeobox gene. This gene is expressed specifically in two food-sensitive chemosensory neuron pairs, AWC and ASE, where it is required for normal expression levels of functionally essential genes, including chemoreceptors and ion channel subunits required for chemotransduction (Lanjuin *et al.*, 2003; Koga and Ohshima, 2004). We found that *ceh-36* worms were nevertheless able to distinguish H from M food, as even untrained worms exhibited a marked preference for the former (Fig. 2B, *che-36*, Untrained vs. $I = 0$, Supplemental Table 1[3]). Moreover, this level of preference was indistinguishable from that exhibited by untrained N2 worms (Fig. 2B, Trained or Untrained *ceh-36* vs. N2, Untrained, Supplemental Table 1[4,5]). However, training had no detectable effect on food preference in *ceh-36* worms (Fig. 2B, *ceh-36*, Trained vs. Untrained, Supplemental Table 1[6]). Taken together, these results show that undiminished *ceh-36* function is required for normal food quality learning, implicating AWC and/or ASE in this process; however, full *ceh-36* function is dispensable for latent food preferences, suggesting the other chemosensory neurons may subserve this behavior.

We next considered the mechanism of accumulation in food patches and how it may be altered by explicit food quality learning. The number of worms in a food patch depends on the difference between their patch entry and exit rates. In a simple experiment to study the effects of entry rate on preference index, we added a fast-acting metabolic poison (sodium azide) to each food patch to prevent worms from leaving (Choi *et al.*, 2016). (To increase the resolution of our preference measurements, we used a T-maze baited with H and M foods (Supplemental Fig. 1). The T-maze prevents worms from wandering out of range of the food spots.)

Trained N2 worms tested in the absence of sodium azide preferred H food to M food more strongly than untrained worms (Fig. 2C, Azide –, Trained vs. Untrained, Supplemental Table 1[7]) indicating a significant effect of food quality training. In the presence of sodium azide, trained and untrained worms still accumulated more strongly in H food than in M food (Fig. 2C: Azide+, Trained and Untrained vs. $I = 0$, Supplemental Table 1[8,9]). This finding shows that preferences can be established on the basis of entry rate alone. The decision to accumulate in a particular food can be made, at least in part, before the animal enters the patch. We also observed a significant effect of training on food preference in the azide condition (Fig. 2C, Azide+, Trained vs. Untrained, Supplemental Table 1[10]), indicating explicit food quality learning increases entry rate. Finally, preference levels were substantially reduced by sodium azide (Fig. 2C, Trained, Azide+ vs. Azide–; Supplemental Table 1[11] and Untrained, Azide+ vs. Azide–; Supplemental Table 1[12]). This result shows that additional mechanisms contribute to differential accumulation in H and M food, mostly likely differences in exit rate, shown previously to contribute to accumulation in open-field accumulation assays (Shtonda and Avery, 2006).

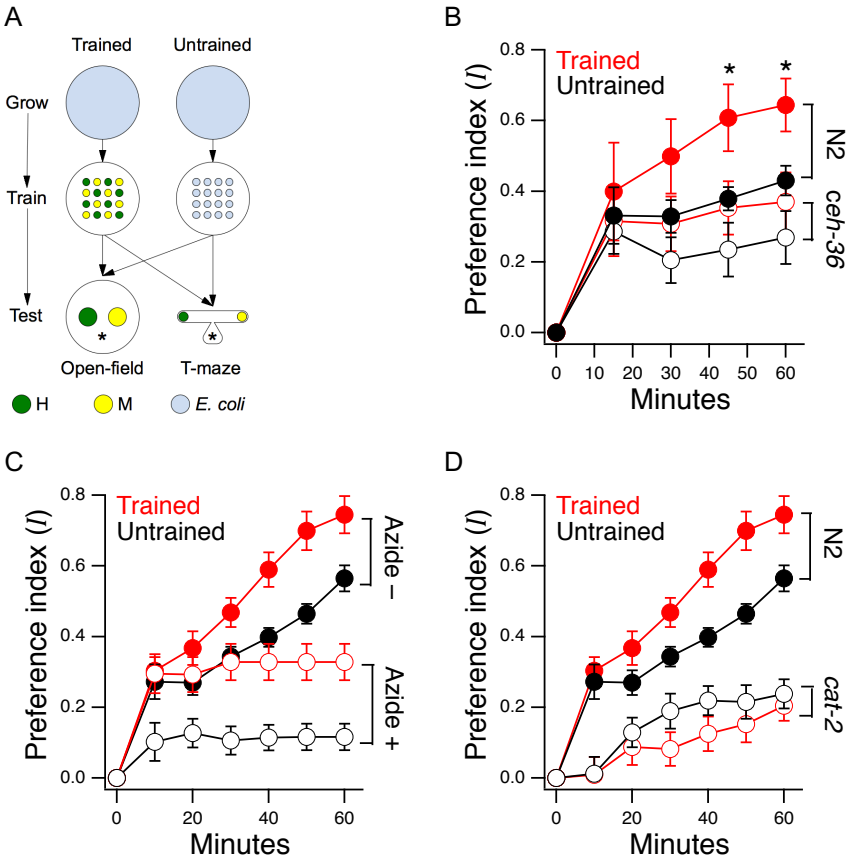

Figure 2. Edible bacteria act as goods over which worms form preferences through experience

A. Food quality training and preference assays. *Filled circles* represent patches of bacteria as indicated in the key. *Stars* indicate worm starting locations. **B**. Mean preference versus time for trained and untrained *ceh-36* mutants and N2 controls in open-field accumulation assays. *Stars*: significant difference between N2 Trained and Untrained (*post hoc t*-test).
C. Mean preference vs. time for trained and untrained N2 worms in T-maze accumulation assays, with and without sodium azide in the food patches. **D**. Mean preference index vs. time for trained and untrained *cat-2(m2261)* mutants and N2 controls in T-maze accumulation assays. N2 data are from C. **A-D**. Error bars ± SEM.

Explicit food quality learning in *C. elegans* is formally equivalent to a type of classical conditioning in which an association is formed between the mélange of odors characteristic of particular bacteria species (Worthy, Haynes, *et al.*, 2018; Worthy, Rojas, *et al.*, 2018) acting as a conditioned stimulus, and their quality as a food source, acting as an unconditioned stimulus. Learning to avoid the odors of pathogenic bacteria is reinforced by serotonin (Zhang, Lu and Bargmann, 2005), but less is known about how preferences for palatable foods are reinforced.

We found that food quality learning is impaired in *cat-2* mutants, which have substantially reduced levels of dopamine (Lints and Emmons, 1999; Sawin, Ranganathan and Horvitz, 2000; Calvo *et al.*, 2011). Preference for H food in untrained *cat-2* mutants was lower than in untrained N2 (Fig. 2D, Untrained, N2 vs. *cat-2*, Supplemental Table 1[13]) indicating an impairment in latent learning. In addition, preference for H food in trained *cat-2* mutants was lower than in trained N2 worms (Fig. 2D, Trained, N2 vs. *cat-2*, Supplemental Table 1[14]), indicating an impairment in explicit learning. Finally, preferences in trained and untrained *cat-2* mutants were indistinguishable (Fig. 2D *cat-2*, Trained vs. Untrained, Supplemental Table 1[15], another indication that explicit learning was impaired.

What accounts for these impairments? Worms move more slowly when in contact with food particles, an effect caused by mechanical activation of dopaminergic neurons (Sawin, Ranganathan and Horvitz, 2000; Tanimoto *et al.*, 2016). Slowing is diminished in *cat-2* mutants (Sawin, Ranganathan and Horvitz, 2000; Cermak *et al.*, 2020), which could cause them to exit the patch sooner than wild type worms. It is possible, therefore, that food quality learning in *cat-2* mutants is impaired simply because they spend less time in the food, hence have less experience of it. However, we found no differences between wild type and *cat-2* mutants in the proportion of time on food (Supplemental Fig. 2). This finding points to a requirement for dopamine signaling in the acquisition or expression of food memory, in accordance with substantial evidence showing a requirement for dopamine in other forms of associative learning in *C. elegans* (Hukema, Rademakers and Jansen, 2008; Voglis and Tavernarakis, 2008; Lee, Jee and McIntire, 2009; Musselman *et al.*, 2012).

GARP prerequisite (ii): quantification of consumption at particular prices. Bacteria are ingested via the worm's pharynx, a rhythmically active muscular pump comprising the animal's throat. Each pharyngeal contraction is called a "pump." In *C. elegans* feeding decisions, the muscular energy utilized while feeding can be thought of as the functional equivalent of money or time in human budgetary experiments. Following this logic, price P can be defined as the energy required to swallow the amount of bacteria ingested in a single pump, $P = e/m$, where e and m are joules per pump and grams of bacterial swallowed per pump, respectively. We propose m is proportional to the optical density d of the offered bacteria suspension. Accordingly, we modeled price of bacteria species X as

$$P_{\mathrm{X}}(d_{\mathrm{X}}, z_{\mathrm{X}}) = e/(z_{\mathrm{X}}\, d_{\mathrm{X}}), \tag{1}$$

where z_{X} is a constant that converts bacteria density into grams per pump. This constant that takes into account several factors: the cellular mass of the bacteria species X (grams/cell), the number of cells that enter the pharynx per unit of optical density (cells/OD), and the fraction of cells entering the pharynx that are passed to the gut. Equation 1 can be converted to relative price p_{X} by that noting energy per pump should be independent of which bacteria species is being consumed, so we can set $e = 1$. Furthermore, as H and M bacteria do not vary greatly in size (Avery and Shtonda, 2003), we made the simplifying assumption that $z_{\mathrm{H}} = z_{\mathrm{M}} = 1$, yielding relative price

$$p_{\mathrm{X}}(d_{\mathrm{X}}) = 1/\, d_{\mathrm{X}}. \tag{2}$$

We modeled the quantity Q of bacteria species X consumed in a feeding bout as

$$Q_{\mathrm{X}}(n_{\mathrm{X}}, z_{\mathrm{X}}, d_{\mathrm{X}}) = n_{\mathrm{X}}\, z_{\mathrm{X}}\, d_{\mathrm{X}}, \tag{3}$$

where n_{X} is the number of pumps in food X. With $z_{\mathrm{X}} = 1$ as above, relative consumption is

$$q_{\mathrm{X}}(n_{\mathrm{X}}, d_{\mathrm{X}}) = n_{\mathrm{X}}\, d_{\mathrm{X}}. \quad (4)$$

For application of GARP, we computed the fractional consumption of each food, q'_{X}, based on the fraction of pumps spent on food X and its density in each choice set,

$$q'_{\mathrm{X}}(f_{\mathrm{X}}, d_{\mathrm{X}}) = f_{\mathrm{X}}\, d_{\mathrm{X}}, \quad (5)$$

where $f_{\mathrm{X}} = n_{\mathrm{X}}/(n_{\mathrm{H}} + n_{\mathrm{M}})$ and n_{H} and n_{M} are, respectively, the number of pumps in H and M food.

To measure the relationship between price and consumption, we developed a system for presenting single worms with a pair of bacteria suspensions while recording the number of pumps the worm “spends” on each (Fig. 3). The system is based on a microfluidic chip (called the "Y-chip" because of its shape) originally created to investigate the neural mechanism of klinotaxis (McCormick *et al.*, 2011), a common form of chemotaxis. *C. elegans* klinotaxis takes the form of accentuating or attenuating, respectively, locomotory head bends toward or away from attractive tastes and odors, including food (Iino and Yoshida, 2009). The Y-chip restrains the worm at the border between two liquid suspensions of bacteria (Fig. 3A,B), representing contiguous patches of food as might occur in the natural environment (Frezal and Felix, 2015). Restraint is achieved by means of a vacuum activated clamp that leaves the worm’s head, upper body, and tail free to move. The worm’s head alternates between the two streams, making sinusoidal movements that resemble crawling on a standard agarose substrate in terms of form and frequency (Supplemental Video 1).

Large movements of the worm’s head in the Y-chip made it impractical to count accurately the number of pumps in a feeding bout by optical methods (Fang-yen, Avery and Samuel, 2009; Scholz *et al.*, 2016). Instead, we counted pumps by simultaneously recording each worm’s electropharyngeogram (Raizen and Avery, 1994) via electrodes inserted into the chip (Lockery *et al.*, 2012). Despite movements of the worm’s body, normal looking EPGs were obtained, with readily identifiable excitation spikes (E) and relaxation spikes (R) (Fig. 3D). We quantified consumption of H and M food in terms of the number of pumps that occurred in each food during a 12-minute exposure to particular food offerings.

GARP prerequisite (iii): decisions from intersecting choice sets: The geometry of the Y-chip enforces the required trade-off between goods. Every swallow that occurs in H food is one that cannot occur in M food, and conversely. By systematically altering the relative concentrations of bacteria on each side of the Y-chip, we could thus alter the relative “prices” of the two kinds of bacteria (number of cells obtained per pump). This allowed us to create a series of choice sets involving different trade-off conditions, and to alter price by varying the concentrations of bacteria. In the experiments presented below we constructed choice sets that intersect, like the choice sets in Fig. 1.

Basic feeding decisions are preserved in Y-chip

A concern at the outset was the possibility that feeding in the Y-chip is not representative of feeding under standard laboratory conditions such as on agar substrates or in liquid culture. For example, the vacuum clamp likely produces mechanical stimulation, which is known to inhibit feeding (Keane and Avery, 2003). It was necessary, therefore, to assess the degree to which feeding behavior in the chip is normal. We did this by comparing the worm’s choices of what to eat and how avidly to eat it on agar plates and in the Y-chip.

Food familiarity effect. *C. elegans* pumps more rapidly in the presence of familiar bacteria than it does in the presence of unfamiliar bacteria (Song *et al.*, 2013). This effect is the result of feeding suppression triggered by the taste or smell of unfamiliar bacteria. To test for this effect in the Y-chip, we grew worms on H food or M food until young adulthood and measured pumping rates either in the same (familiar) or the converse (unfamiliar) food. We found that mean pumping rate for a given type of food was higher when that food was familiar, indicating that this aspect of feeding is intact in the Y-chip (Fig. 4A, Familiar food vs. Unfamiliar food, Supplemental Table 1[16]). Further, we noted that pumping rate in familiar food happened to be the same regardless of which food was familiar, allowing us to directly compare the extent to which unfamiliar food suppressed pumping rate. Interestingly, suppression was greater when the unfamiliar food

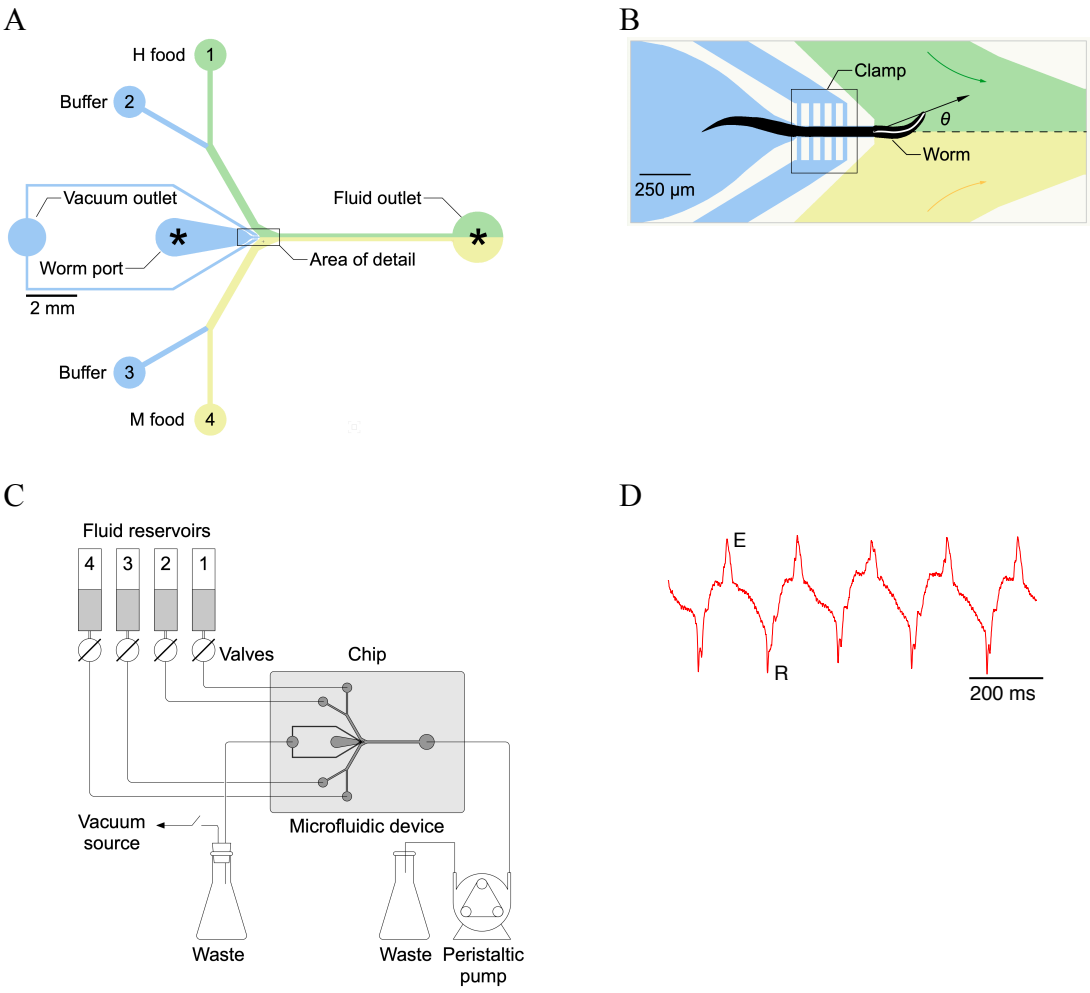

Figure 3. Single-worm food choice assays

A. Layout of the Y-chip. *Asterisks* indicate the position of recording electrodes. Ground electrodes (not shown) were inserted into the food and buffer ports to reduce electrical interference. The chip is shown configured for the experiments in Figs. 4B and 5B. **B**. Area of detail shown in B. The dashed line is the centerline of chip; the white line within the worm is its centerline. The black arrow connects the middle of the neck where it enters the food channel with anterior end of worm's centerline. Positive values of head angle (θ) indicate displacement toward H food. Colored arrows show direction of flow. **C**. Schematic overview of fluidic system. **D**. Typical electropharyngeogram. Each pair of excitation (E) and relaxation (R) spikes constitutes one pharyngeal pump.

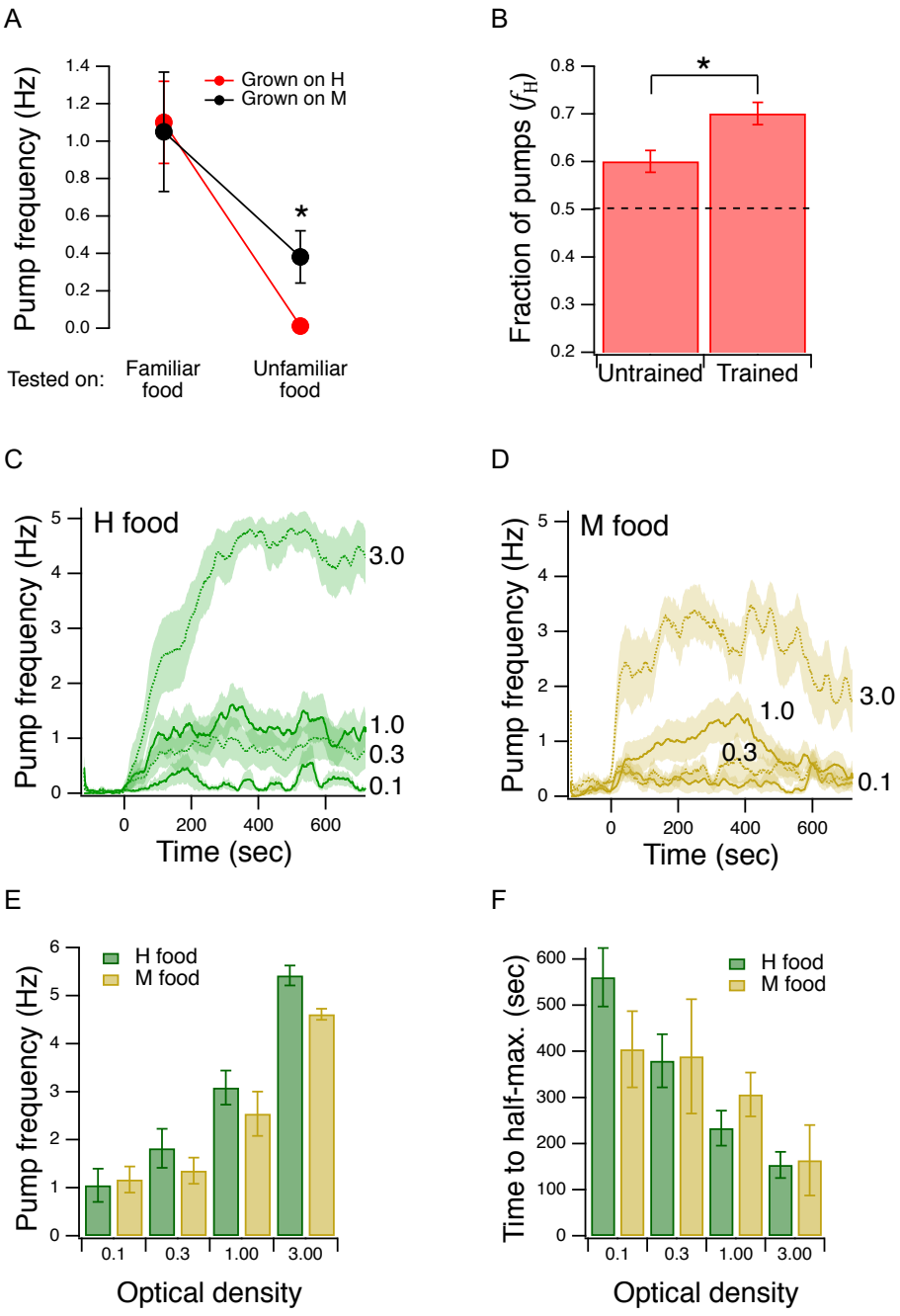

Figure 4. Validation of the Y-chip for measuring food preferences

A. Familiar food effect. Mean pump frequency of worms grown on H or M food and tested on the same or the other type of food. Both foods were at OD 1. Pumping was recorded for 12 min. **B**. Food quality learning. Mean fraction of pumps in H food in trained and untrained worms. The *dashed line* indicates equal preference for H and M food. Both foods were at OD 1. **C,D**. Time course of pump frequency at four different food densities. The optical density is indicated next to each trace. **E**. Dependence of mean pump frequency on food density. **F**. Dependence of latency to half-maximal pump frequency on food density. **A-F**. Error bars and shading ± SEM.

was lower in quality than the familiar food (Fig. 4A, Unfamiliar food, grown on H vs. grown on M, Supplemental Table 1[17]). This result is consistent with a model in which worms are even more reluctant to feed on unfamiliar food when it is worse than what they have eaten in the recent past. A similar result has been seen in the case of food-patch leaving behavior (Shtonda and Avery, 2006).

Explicit food quality learning. We tested groups of trained and untrained worms with H and M food at equal concentrations (OD 1.0) in the Y-chip. Preference, as indicated by the fraction of pumps in H food (f_{H}, see Methods), in trained and untrained worms was greater than 0.5, indicating they preferred H food in the chip, just as they do in accumulation assays (Fig. 4B, Supplemental Table 1[18,19]). Moreover, we found that this preference was enhanced by training, again consistent with accumulation assays (Fig. 4B, Trained vs. Untrained, Supplemental Table 1[20]). We conclude that explicit food quality learning is intact in the Y-chip.

Effect of food density on pumping rate. Although there appear to be no systematic studies of this effect when worms are feeding on bacteria lawns in petri plates, pumping rate has been shown to increase as a function of food density in liquid culture (Avery and Horvitz, 1990). This effect has also been demonstrated under conditions of mild restraint in microfluidic devices (Scholz *et al.*, 2016; Lee *et al.*, 2017; Weeks *et al.*, 2018) To test for this effect in the Y-chip, we trained worms as in Fig. 2A, except that the training plate contained a single food, H or M. During testing, both channels in the Y-chip carried the food on which the animals were trained (H or M) at an OD of 0.1, 0.3, 1.0, or 3.0. Pumping rate in H food was stable whereas pumping rate in M appeared to decline later in the experiment (Fig. 4C,D); accordingly, we quantified pumping in terms of its peak rate for both food types. Peak pumping rate was comparable to the rate recorded in similar concentrations of *E. coli* strain OP50 under mild restraint in microfluidic devices (Scholz *et al.*, 2016; Lee *et al.*, 2017; Weeks *et al.*, 2018), and exhibited the expected increase with food density (Fig. 4E; main effect of OD, Supplemental Table 1[21]). We conclude that the concentration dependence of pumping rate is intact in the Y-chip. This experiment also revealed previously unreported aspects of pumping kinetics. Regardless of food type, pumping rate rose slowly, on the time scale of 100s of seconds (Fig. 4C,D), Additionally, we observed an inverse relationship between the latency to half-maximum pumping rate and concentration (Fig. 4F; Half-time vs. OD, Supplemental Table 1[22]). Thus, worms encountering a richer food source eat sooner at higher rates, a coordinated response that is presumably adaptive in natural environments.

Demand curves

We next turned to the central question of whether *C. elegans* feeding behavior is altered by the relative price of food options that vary in quality. Economists identify several different types of goods according to how demand (or equivalently, consumption) is affected by changes in income or price. An *ordinary* good is one for which there is an inverse relationship between price and demand. To determine whether H and M food behave as ordinary goods in *C. elegans* feeding ecology, we constructed *demand curves*, in which relative consumption q_{X} was plotted against relative price p_{X} for H and M food (Fig. 5A). We found an inverse relationship between mean consumption and price, indicating that H and M food do act as ordinary goods, well suited to a GARP experiment.

More broadly, these results show that *C. elegans* obeys the classic law of demand, exhibiting the fundamental sensitivity of consumption to price seen in humans. The data of Fig. 5A were well fit by

$$q_{\mathrm{X}}(p_{\mathrm{X}}) = A{p_{\mathrm{X}}}^{\epsilon}, \qquad (6)$$

where A is a positive constant and $\epsilon < 0$. This is the equation for a demand curve in which the sensitivity of consumption to changes in price is constant at all prices, i.e., there is constant *elasticity of demand* (Varian, 1992). We found $\epsilon \cong -2$ for both food types, indicating strong elasticity, a condition that arises when there many goods of nearly equivalent utility in the market. Interestingly, this may actually be the case for *C. elegans*, which grows robustly on approximately 80% of the hundreds of bacteria species in its natural habitat (Samuel *et al.*, 2016). Elasticity is not always the case in foraging animals. Rats exhibit inelastic demand ($-1 < \epsilon < 0$) when offered only essential commodities such as food pellets and water (Kagel *et al.*, 1975, 1981).

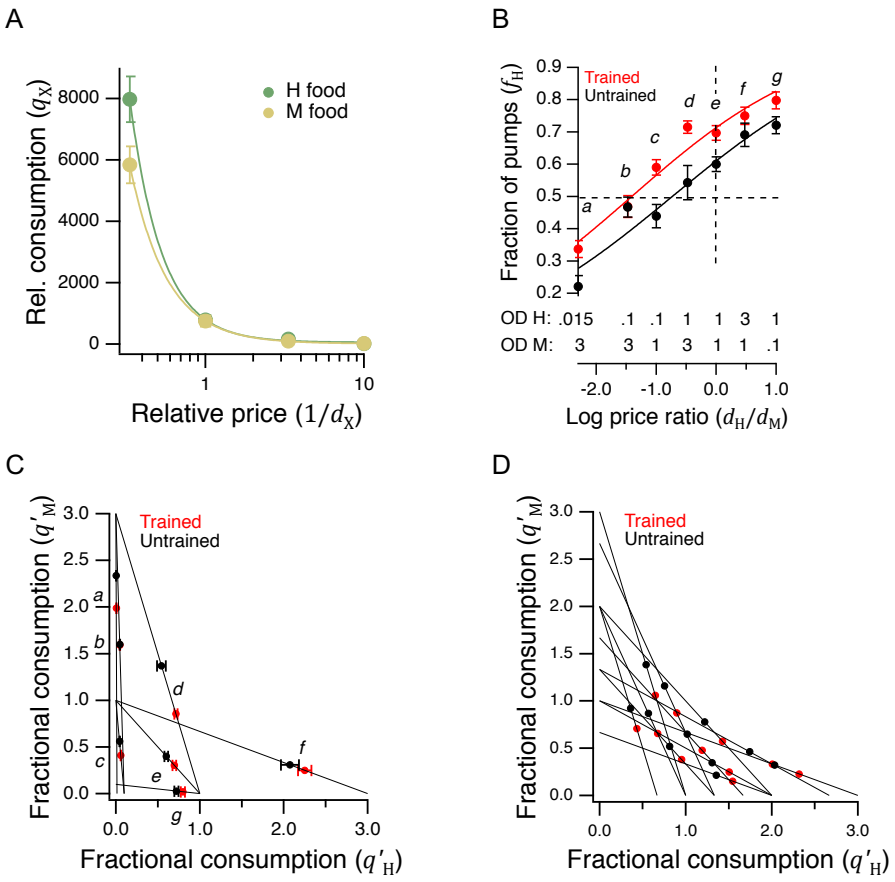

Figure 5. Economic analysis of food choice in *C. elegans*

A. Demand curves. Mean relative consumption of familiar food versus its relative price. The data are fit by equation 6 with $\epsilon = -2.2$ for H food and $\epsilon = -1.9$ for M food. **B**. Price ratio curves. Food preference, measured as fraction of pumps in H food, versus price ratio for Trained and Untrained worms. *Horizontal dashed line*: indifference between H and M food; *vertical dashed line*: H and M food at equal price. Data at log price ratio = 0 are replotted from Fig. 4B. **C**. GARP analysis of *C. elegans* food preferences. Plotted points show mean consumption of M food versus consumption of H food in Trained and Untrained worms. Lines are choice sets as in Fig. 1. The x and y intercepts of each line indicate the amounts of H and M food that would have been consumed if the worm spent all its pumps on one or the other food type. **D**. Predicted consumption of H and M food in Trained and Untrained animals on the a widely-used ensemble containing 11 budget lines (Harbaugh, Krause and Berry, 2001). **A-C**. Error bars ± SEM.

Integration of preference and price

In a GARP experiment, participants evaluate offerings in the choice sets by integrating their preferences with constraints driven by prices. To determine if *C. elegans* performs a similar integration, we repeated the experiment of Fig. 4B, now for a broad range of relative H and M prices. To avoid progressive effects of feeding and satiety on food choices, each worm experienced a single choice set, and we allowed worms to feed for only 12 minutes.

Data were analyzed by plotting the mean fraction of pumps spent on H food, f_{H}, against the log of price ratio $log(p_{\mathrm{M}}/p_{\mathrm{H}})$ which, by equation 2, is equal to $log(d_{\mathrm{H}}/d_{\mathrm{M}})$. The data were fit by an exponential sigmoid function of the form

$$f_{\mathrm{H}}(r) = 1/(1 + 10^{-(r-r_o)/k}), \quad (7)$$

where r is log price ratio, r_0 is log price ratio at the point of indifference between H and M food ($f_{\mathrm{H}}(r_0) = 0.5$) , and k is the dynamic range of the function. We chose an exponential sigmoid because, like f_{H}, it is bounded between 0 and 1. We refer to this mathematical relationship as a *price-ratio curve*. We found that worms spent more pumps on H food as its relative density rose, i.e., as its relative price was reduced (Fig. 5B, effect of price ratio, Supplemental Table 1[23]), and training shifted the price-ratio curve upward (Fig. 5B, Trained vs. Untrained, Supplemental Table 1[24]). Importantly, however, we also found that worms could be induced to spend the majority of pumps on M food if the H food was made sufficiently dilute, i.e., expensive (Fig. 5B, point *a*, Trained and Untrained, $f_{\mathrm{H}} < 0.5$, Supplemental Table 1[25,26]). Taken together, these data show that neither food preference nor price is the sole determining factor for consumption. Instead, worms appear to take both preference and price into account, as human consumers often do, and as required for a GARP experiment.

Utility maximization

To apply the formal test for utility maximization to *C. elegans* food choice, we mapped the data of Fig. 5B into the GARP framework by plotting mean consumption of M food against mean consumption of H food at each price ratio (Fig. 5C). Under this mapping, the lines in Fig. 5C correspond to choice sets like those in Fig. 1. There is one line for each price ratio. The x and y intercepts of these lines indicate the amount of food (up to a scale factor) that would have been consumed had the worms spent all of their pumps on H or M food, respectively. We found it impractical to standardize the number of pumps to impose a fixed energy budget on each worm because of individual differences in latency to feed and mean pumping rate during the recordings (Fig. 5B). We therefore plotted mean fractional consumption, q'_{H} and q'_{M} (equation 5). However, it is unlikely that standardization would have significantly changed experimental outcomes because the relative number of pumps in each food type was stable throughout the recording period (data not shown).

Following the standard method from economics, utility maximization was formally assessed according to the procedure outlined by Varian (Varian, 1995). This assessment yields a single number that captures the total degree of consistency of preferences. It revealed no violations in either the trained or untrained data set (Fig. 5B). We provisionally concluded that worms were choosing precisely as if they were maximizing utility on the seven budget lines in our study.

To assess the robustness of our finding of utility maximization, we first considered whether it could be attributed to sampling error. Error bars in Fig. 5C show the standard error of the mean for consumption of H food on each budget line. Given this variability, it is conceivable that one or more violations was missed because of sampling error. We therefore constructed 10^8 simulated data sets by sampling from gaussian distributions implied by the aforementioned standard errors. Finding no violations of utility maximization in either the trained or untrained group in multiple trials, we estimate the probability of at least one violation to be less than 10^{-8}. It is therefore unlikely that the absence of violations was an accident of sampling error.

However, it is conceivable that violations might have been observed if we had used a larger ensemble of budget lines. To address this concern, we predicted the choices worms would make on a widely used ensemble (Harbaugh, Krause and Berry, 2001; Camille *et al.*, 2011; Chung, Tymula and Glimcher, 2017), which contains 11 budget lines and covers the choice space more uniformly than our 7-budget ensemble. We first assessed the stringency of the 11-budget ensemble as a test for the utility maximization. This was done by assuming a highly conservative null hypothesis: that worms choose completely randomly, such that the fraction of pumps in H food, f_{H}, is drawn from a flat distribution between 0 and 1 (fraction of pumps in M food was $1 - f_{\mathrm{H}}$). Based on 10^6 random data sets constructed in this way, we estimate the probability of a false positive finding of utility maximization (no violations) in the 11-budget ensemble to be 0.06. The 7-budget ensemble, by comparison, has a false positive probability of 0.87. We conclude that the 11-budget ensemble is sufficiently stringent.

To compute how *C. elegans* would be expected to perform when choosing on the 11-budget ensemble we used equation 7 to predict the expected behavior on the budget lines in Fig. 5D. Separately, we also used piecewise linear representations of Fig. 5B data (not shown). In both cases we assumed that: (i) f_{H}, the fraction of pumps in H food is determined by relative food density, with no contribution from absolute amounts of either food and (ii) that f_{H} is a smooth function of price ratio, to the extent implied by either type of fit. Partial support for assumption (i) comes from the observation that the highest preference observed in this study (Fig. 5A, point *g*) was obtained with mid-range optical densities. To be conservative, we sampled f_{H} at each price ratio according the maximum standard error of the mean in the corresponding data set in Fig. 5B (Trained or Untrained). The probability that worms would exhibit utility maximization in the 11-budget ensemble was ≥ 0.98, regardless of training state or type of fit (equation 7 or piecewise linear). We conclude that the worm's price-ratio curve likely constitutes a robust utility maximization strategy.

Higher order features of utility maximization. Evidence that *C. elegans* is a utility maximizer (Fig. 5C, D), allowed us to investigate higher order features of utility maximization considered to be properties of human decisions. Ultimately, we succeeded in establishing a utility model describing what may be the underlying valuation process guiding the worm's choices.

Economic theory distinguishes between two main classes of goods – *substitutes* versus *complements* – according to how changes in the price or quantity of one good that a consumer possesses affects consumption of a second good. In the case of substitutes, which are defined as being more or less interchangeable from the consumer's perspective, an increase in the price of one good causes a decrease in the consumption of that good and a compensatory increase in consumption of the other good. This occurs as consumers trade some of the good whose price increased for more of the alternative good. Pairs of goods that are traded-off at a constant exchange rate, regardless of the amounts of goods on offer, are called *perfect substitutes*; black and blue pens are an example of perfect substitutes (if color is not a deciding factor). In the case of complements, which are defined as goods that are more desirable when consumed together rather than separately, an increase in the price of one good causes a decrease in consumption of both goods. Left and right shoes of the same style and size are an example of perfect complements. Wearing only one shoe has essentially zero utility, so increases in the price of left shoes leads to decreased shoe consumption overall. Although *C. elegans* consistently ate some of both foods in our experiments, we predicted that H and M food should act, to some degree, as substitutes for each other, as each provides nutrition.

To test this prediction, we took advantage of the design of the experiment in Fig. 5B. The seven choice sets can be arranged in three groups in which the price of one food was held constant while the other food was offered at three different prices. In particular, there were two groups in which the price of M food was constant while the price H food changed (points *a*, *b*, *d*, and points *c*, *e*, *f*), and there was one group in which the price of H food as constant while the price of M food changed (points *d*, *e*, *g*). We analyzed these instances by plotting consumption of the food whose price was constant against the price of the other food (Fig. 6A). In five out of six cases, consumption of the constant-price food increased in response to increases in the price of the other food (Fig. 6A, non-zero positive slope, Supplemental Table 1[27-32]). We conclude that H and M food are substitutes for *C. elegans* as predicted.

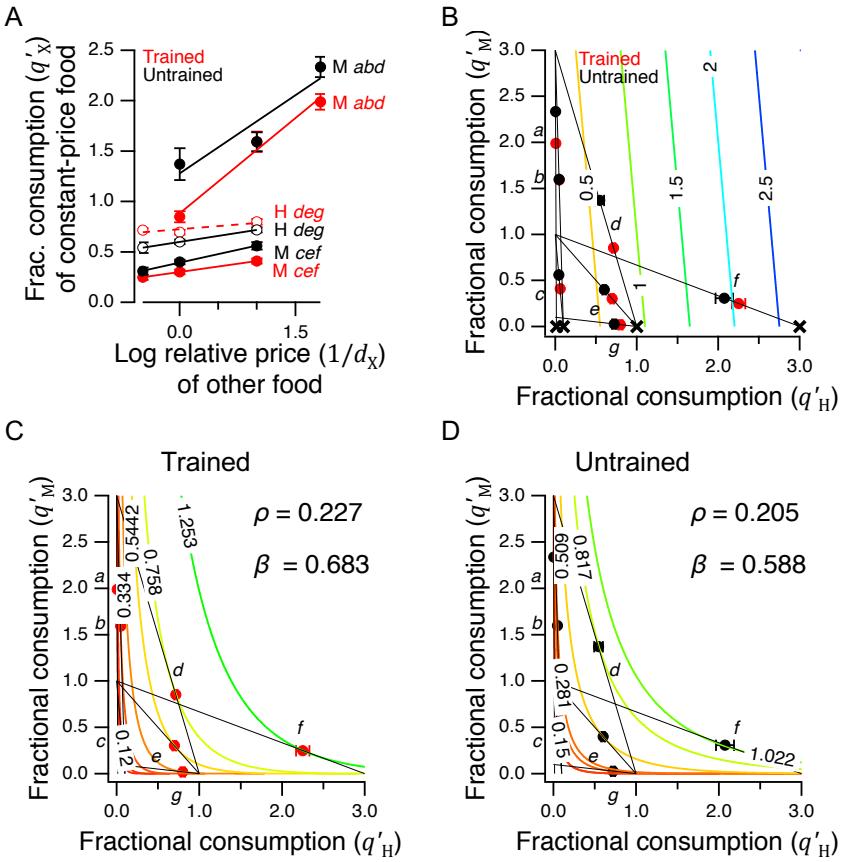

Figure 6. Higher-order features of utility maximization

A. H and M food act as substitutes. Consumption is plotted against price for triplets of cost ratios in which the concentration of one food was constant and the concentration of the other food was variable. *Lower case italic letters*: data points in Fig. 5B. *Capital letters*: the food whose density was constant, the consumption of which is plotted on the y-axis. *Solid lines*: regression slope different from zero ($p \leq 0.01$); d*ashed lines*: slope not different from zero. **B**. H and M food are not perfect substitutes. Colored contour lines are indifference curves in a perfect substitute model (equation 8) with $\beta = 10/11$. Data points from Fig. 5C are replotted for comparison, with associated budget lines, according to the conventions of that figure. 'X' symbols indicate the point of highest utility on each budget line. **C-D**. Best fitting parameterizations of the CES function (equation 9) for Trained and Untrained animals. Each panel shows the seven the iso-utility lines that are tangent to the budget lines. Goodness of fit can be assessed by observing that the iso-utility lines are tangent to the budget lines at, or near, the data points which indicate mean consumption of H and M food, replotted from Fig. 5C. **A-D**. Error bars $\pm$ SEM.

Further, we can be reasonably certain that the H and M foods used in our experiments are not *perfect substitutes*. In the case of perfect substitutes, utility is the weighted sum of the consumed amount of each good. This relationship can be described with the equation

$$U(x, y) = \beta x + (1 - \beta)y, \tag{8}$$

where x and y are the amounts of each good, and β is a weighting factor between 0 and 1 (inclusive). In that case, the exchange rate between the two goods, i.e., the amount of y required to compensate for giving up one unit of x, is a constant, $\beta/(1-\beta)$. For example, goods that can be substituted on a one-for-one basis have an exchange rate of unity ($\beta = 0.5$). Equation 8 defines a planar utility surface that lies above the positive x, y plane and passes through the origin. This plane is indicated by the colored contour lines in Fig. 6B, which also contains the data of Fig. 5C for comparison. The contour lines represent iso-utility lines within the plane. In economics, such lines are called *indifference curves*, because a chooser would be indifferent between bundles located on the same curve, as these bundles would have the same utility. In the example shown, $\beta = 10/11 > 0.5$, meaning that the slope of the plane is steeper in the direction parallel to the axis indicating consumption of good x, i.e, H food in the figure. A utility maximizer will therefore choose the points labeled "X" as these have the highest utility available on the associated budget line. Such points are called *corner solutions*, which are situations when the chooser devotes the entire budget to a one of the two options. Here, the corner solutions are arrayed along the x axis (and a hypothetical worm showing this pattern of perfect substitution would spend all of its pumps eating only the H food); for $\beta < 0.5$ the corner solutions would be arrayed along the y-axis. The complete absence of corner solutions in our data is evidence that *C. elegans* does not perceive H and M food as perfect substitutes under our conditions, but rather as *imperfect substitutes*.

A model of valuation in the worm. In widely used models of choices made by human consumers when offered imperfect substitutes, the exchange rate is not constant, but varies as a function of the amount of each good offered in a particular bundle. In economics this case is often modeled by the Constant Elasticity of Substitution (CES) function. In the present case the CES function takes the form

$$U(q_{\mathrm{H}}, q_{\mathrm{M}}) = (\beta {q_{\mathrm{H}}}^{\rho} + (1 - \beta){q_{\mathrm{M}}}^{\rho})^{1/\rho}. \tag{9}$$

The exponent ρ ($\neq 0$) represents the sensitivity of choosers to the fact that the more of a good they already possess, the less valuable each additional unit of the good becomes; in economics, this is called *diminishing marginal utility*. This sensitivity is inversely related to ρ. Here, as in equation 8, β captures the tradeoff between the goods, now after transformation by ρ. The CES utility function is quite flexible in that it can generate utility surfaces (and hence indifference curves) for perfect substitutes (when $\rho = 1$), imperfect substitutes (when $-0.5 < \rho < 1$), and perfect complements ($\rho \ll -0.5$).

The best fitting parameterizations of the CES function for our data (β, ρ) are shown for trained and untrained worms in Fig. 6C and D, respectively. The highest contour reached by any budget line is the one that is tangent to it, and this contour constitutes the CES function's prediction of the worm's mean preference in that choice set. The close match between model and behavior for trained and untrained worms indicates that *C. elegans* food choice conforms to a widely used model of choice behavior in humans. The fact that β increased shows that after training the relative value of H food was higher than before. The fact that ρ increased (became more positive) indicates that worms became less sensitive to diminishing marginal utility. Thus, not only did training make H food more attractive, it also made worms require more of it to be satisfied.

Behavioral mechanisms of utility maximization

Having shown that the worm's preferences are consistent with utility maximization and, like human preferences, modeled by the CES function, we next asked how utility is maximized at the behavioral level. As noted in above, we defined preference as the fraction of pumps in H food, $f_{\mathrm{H}} = N_{\mathrm{H}}/(N_{\mathrm{H}} + N_{\mathrm{M}})$, where N_{H} and N_{M} are the number of pumps in H and M food, respectively. In one model, the behavioral expression of preference is a higher pumping rate in the preferred option (the "pumping-rate model"). Alternatively, it

might be increased amount of time spent feeding on the preferred side (the "dwell-time model"). Because the number of pumps in a given food type is equal to product of the time spent in that food and the mean pumping frequency in that food, an equivalent expression for preference is

$$f_{\mathrm{H}} = \frac{F_{\mathrm{H}} t_{\mathrm{H}}}{F_{\mathrm{H}} t_{\mathrm{H}} + F_{\mathrm{M}} t_{\mathrm{M}}} \tag{10}$$

where F and t are, respectively, mean pumping frequency and mean total dwell time in the indicated food type. Limiting cases are informative here. If preference depends entirely on pumping frequency, then $t_{\mathrm{H}} = t_{\mathrm{M}}$, and equation 10 reduces to the pumping-rate model

$$f_{\mathrm{H}} = \frac{F_{\mathrm{H}}}{F_{\mathrm{H}} + F_{\mathrm{M}}} \tag{11}$$

in which preference for H food occurs when $F_{\mathrm{H}} > F_{\mathrm{M}}$, whereas preference for M food occurs when $F_{\mathrm{M}} > F_{\mathrm{H}}$. Plotting preference as defined by equation 11 for each animal against its actual preference, $f_{\mathrm{H}} = N_{\mathrm{H}}/(N_{\mathrm{H}} + N_{\mathrm{M}})$, revealed a modest but significant negative correlation (Fig. 7A, Supplemental Table 1[33]). This result indicates a paradoxical but weak tendency to pump more slowly in H food as preference for it increases. Conversely, if preference depends entirely on time in each food, then $F_{\mathrm{H}} = F_{\mathrm{M}}$, and equation 10 reduces to the dwell-time model

$$f_{\mathrm{H}} = \frac{t_{\mathrm{H}}}{t_{\mathrm{H}} + t_{\mathrm{M}}} \tag{12}$$

in which preference for H food occurs when $t_{\mathrm{H}} > t_{\mathrm{M}}$, whereas preference M food occurs when $t_{\mathrm{M}} > t_{\mathrm{H}}$. Consistent with the dwell time model, we found a strong positive correlation between preference as defined by equation 12 and actual preference (Fig. 7B, Supplemental Table 1[34]). Together, these findings eliminate the support the dwell-time model and exclude the frequency model.

To determine how dwell time is biased toward the preferred food option, we measured mean head angle for each animal in the data set underlying Fig. 5B. As expected, we found a strong positive correlation between preference defined by equation 12 and mean head angle in the Y-chip (Fig. 7C, Supplemental Table 1[35]). Calcium imaging suggests that the angle of the worm's head with respect to the rest of the body is regulated by differential activation of dorsal and ventral neck muscle motor neurons (Hendricks *et al.*, 2012). We propose, therefore, that the function of the neural circuit that maximizes utility is to generate asymmetric activation of these motor neurons during head bends.

Role of chemosensory neurons in utility maximization

In a final series of experiments we began the search for neuronal representations of utility in *C. elegans*, beginning with its chemosensory neurons.

ceh-36 is required for explicit food quality learning in the Y-chip. As shown in Fig. 4B, N2 worms preferred H to M food in the Y-chip, and there was a significant effect of training. In the experiment of Fig. 7D, we found that whereas untrained *ceh-36* worms also preferred H to M food (Fig. 7D, *ceh-36* Untrained, $f_{\mathrm{H}} > 0.5$, Supplemental Table 1[36]), the effect of food quality training differed between N2 and *ceh-36* (Fig. 7D, training × strain, Supplemental Table 1[37]), such that trained and untrained *ceh-36* worms were indistinguishable (Fig. 7D, *ceh-36* Trained vs. Untrained, Supplemental Table 1[38]). These findings indicate an absolute requirement for normally function in the *che-36* expressing neurons AWC and/or ASE in food quality learning.

Characterization of AWC's response to delivery and removal of bacteria. We next performed a series of calcium imaging experiments to characterize the worm's internal representations of H and M food. We focused on AWC because it is one of the few chemosensory neuron classes known from optogenetic manipulation to be capable of producing precisely the type of head-angle bias that underlies the expression of utility maximization in *C. elegans* (Fig. 7C)(Kocabas *et al.*, 2012). The two AWC neurons are designated

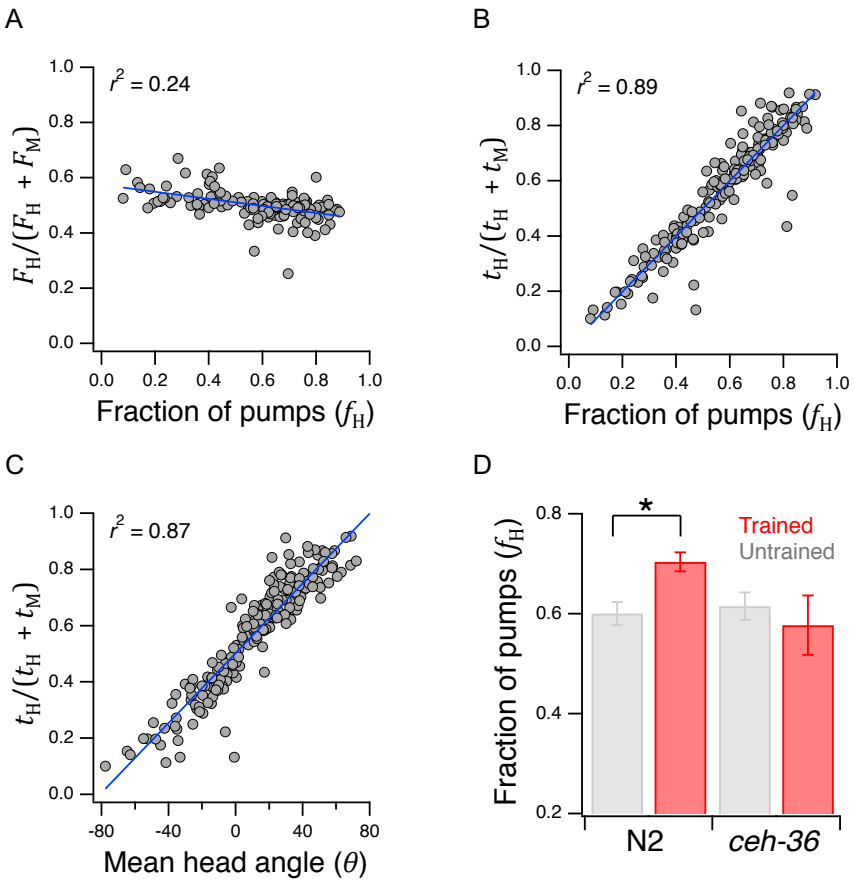

Figure 7. Behavioral mechanisms of utility maximization

A. Pumping-rate model of preference. Equation 11 is evaluated for each worm in Fig. 5B and the result is plotted against preference in terms of fraction of pumps in H food for the same animal. **B**. Dwell-time model of preference. Same as A but using equation 12. **C**. Regression of equation 12 against mean head angle as defined in Fig. 3. **A-C**. *Blue lines*: regressions on the data. **D**. Diminished *ceh-36* function eliminates the effect of food quality training on food preference. H and M are at OD = 1. N2 data are from Fig. 4B. Error bars ± SEM.

AWC^{ON} and AWC^{OFF} according to slight differences in gene expression (Wes and Bargmann, 2001). AWC^{ON} and AWC^{OFF} generate similar calcium transients to odorants that they both detect (Chalasani *et al.*, 2007); for consistency, we recorded from AWC^{ON} (henceforth, "AWC"). Calcium imaging shows that AWC is inhibited by bacteria conditioned medium or odorants, such as isoamyl alcohol, that are released by attractive bacteria (Worthy, Haynes, *et al.*, 2018) but then responds with a robust, positive-going transient when the stimulus is removed. Thus, AWC is widely considered to be food-off neuron. However, in one case, AWC is known to generate an off-transient when the stimulus is switched from the odor of a preferred pathogenic food, *Pseudomonas aeruginosa*, to the odor of a less preferred nonpathogenic food, *E. coli* (Ha *et al.*, 2010). This finding is the first hint that AWC may be an off-neuron with more sophisticated sensitivities; here we provide further evidence of this.

For consistency with conditions of our behavioral experiments (Fig. 2,4,5), we stimulated AWC with suspensions of H and M bacteria. As most previous assessments of AWC's responsivity utilized either bacteria conditioned medium or odorants, we first characterized AWC's responses to the delivery and removal of bacteria. Such events mimic the experience of an AWC neuron when the worm moves in or out of a food patch, respectively, as in our accumulation assays (e.g., Fig. 2B-D). We found, as expected from odorant experiments, that AWC is inhibited by food onset (Fig. 8A) and excited by food offset (Fig. 8C) regardless of food type.

Do AWC responses reflect the worm's overall preference for H? With respect to food onset, the apparently stronger inhibition in response to H than M food, measured as integrated calcium response, did not reach significance (Fig. 8B, effect of food type, Supplemental Table 1[39]). However, with respect to food offset, AWC was more strongly excited by H than M food (Fig. 8D, effect of food type, Supplemental Table 1[40]). At the more fine-grained level of peak responses within training groups, peak H food responses were significantly stronger than peak M food responses (Fig. 8C, Untrained, effect of food type, asterisk, Supplemental Table 1[41]; Fig. 8C, Trained, effect of food type, cross, Supplemental Table 1[42]). Overall, we conclude AWC responds more strongly to removal of H food than M food. As AWC produces a bout of reverse locomotion when activated (Gordus A, Pokala N, Levy S, Flavell SW, 2015), its response to food offset promotes reversals, leading to increased retention patches. Our imaging data suggest that AWC-mediated retention would be stronger for H than M food, promoting greater preference for H food, as seen in Fig. 2B-D.

What is the effect of food-quality training on AWC responses? In the case of food onset, training appeared to strengthen inhibition to H food and weaken inhibition to M food in terms of integrated responses, but this trend did not reach significance (Fig. 8B, effect of training, Supplemental Table 1[43]). In the case of food offset, the results were clearer. There was a main effect of training on integrated calcium transients (Fig. 8D, Trained vs. Untrained, Supplemental Table 1[44]), but this effect was limited to H food (Fig. 8D, H food, Trained vs. Untrained, *, Supplemental Table 1[45, 46]). Overall, our imaging data suggest that AWC-mediated retention in H food patches would be stronger in trained than untrained animals, promoting greater preference for H food after training, as seen in Fig. 2B-D.

Imaging AWC's response to food in Y-chip assays. To mimic the experience of the worm in the Y-chip, we recorded AWC responses to switching directly from one food type to the other. In the first experiment, H and M food were presented at the same optical density (OD = 1). If AWC were merely a food-off neuron, there should no response as food concentration did not change. On the contrary, AWC was strongly excited by H→M transitions, and peak responses were amplified by food-quality training (Fig. 9A, *asterisk*, Trained vs. Untrained, Supplemental Table 1[47]). AWC appeared to be inhibited by M→H transitions. The extent of inhibition, quantified as the integrated calcium transient, was insensitive to training (Fig. 9A, Supplemental Table 1[48]). Overall, we conclude that AWC is capable of reporting more than the presence or absence of food, but also its identity as a preferred high-quality food source.

Taken together, the fact that normal *ceh-36* function is required for food preference in the Y-chip (Fig. 7D), and that AWC is sensitive to food quality (Fig. 9A), suggest that it may provide sensory input to the worm's utility maximization circuit. However, such a neuron must also be shown respond to changes in food value on the time scale of individual head bends. We therefore presented worms with an alternating series of 2 sec step-wise presentations of H then M food. This stimulus pattern mimics the effect on AWC of head

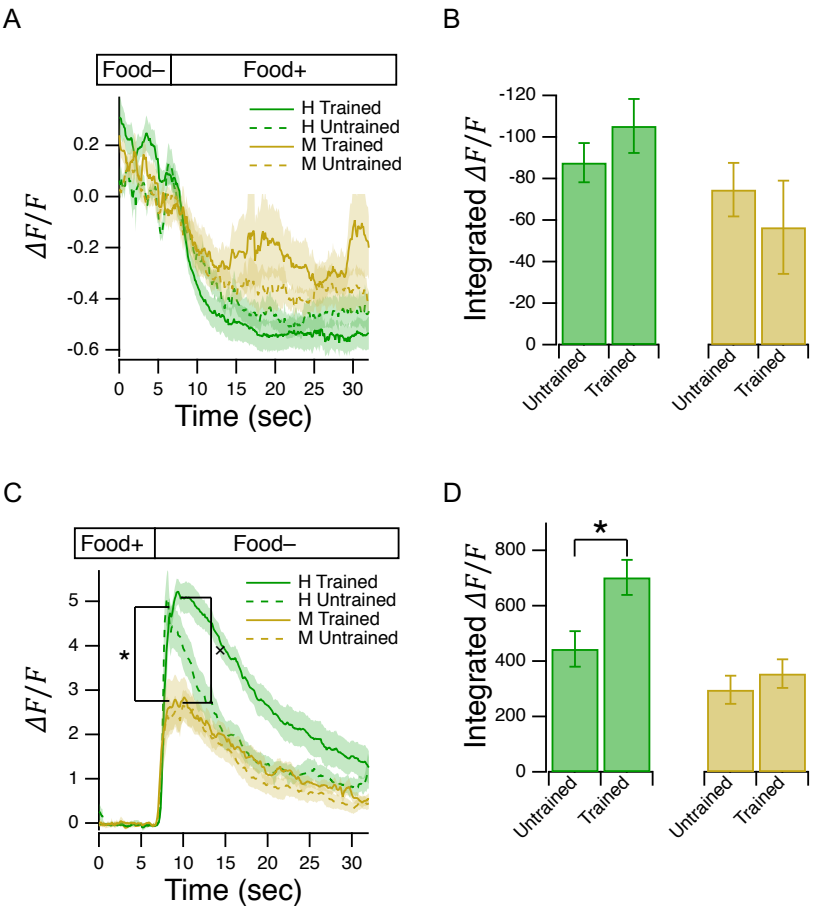

Figure 8. Characterization of AWC's response to delivery and removal of food

A. Ensemble averages of relative fluorescence versus time in response to onset of the indicated food in trained and untrained animals. **B**. Summary of data in A, showing mean integrated calcium transients. **C**. Ensemble averages of relative fluorescence versus time in response to removal of the indicated food in trained and untrained animals. *Asterisk*: untrained group, mean peak response, significant difference H vs. M. *Cross*: trained group, mean peak response, significan difference H vs. M. **D**. Summary of data in C, showing mean integrated calcium transients *Asterisk*: significant difference between means. **A-D**. Shading and error bars ± SEM.

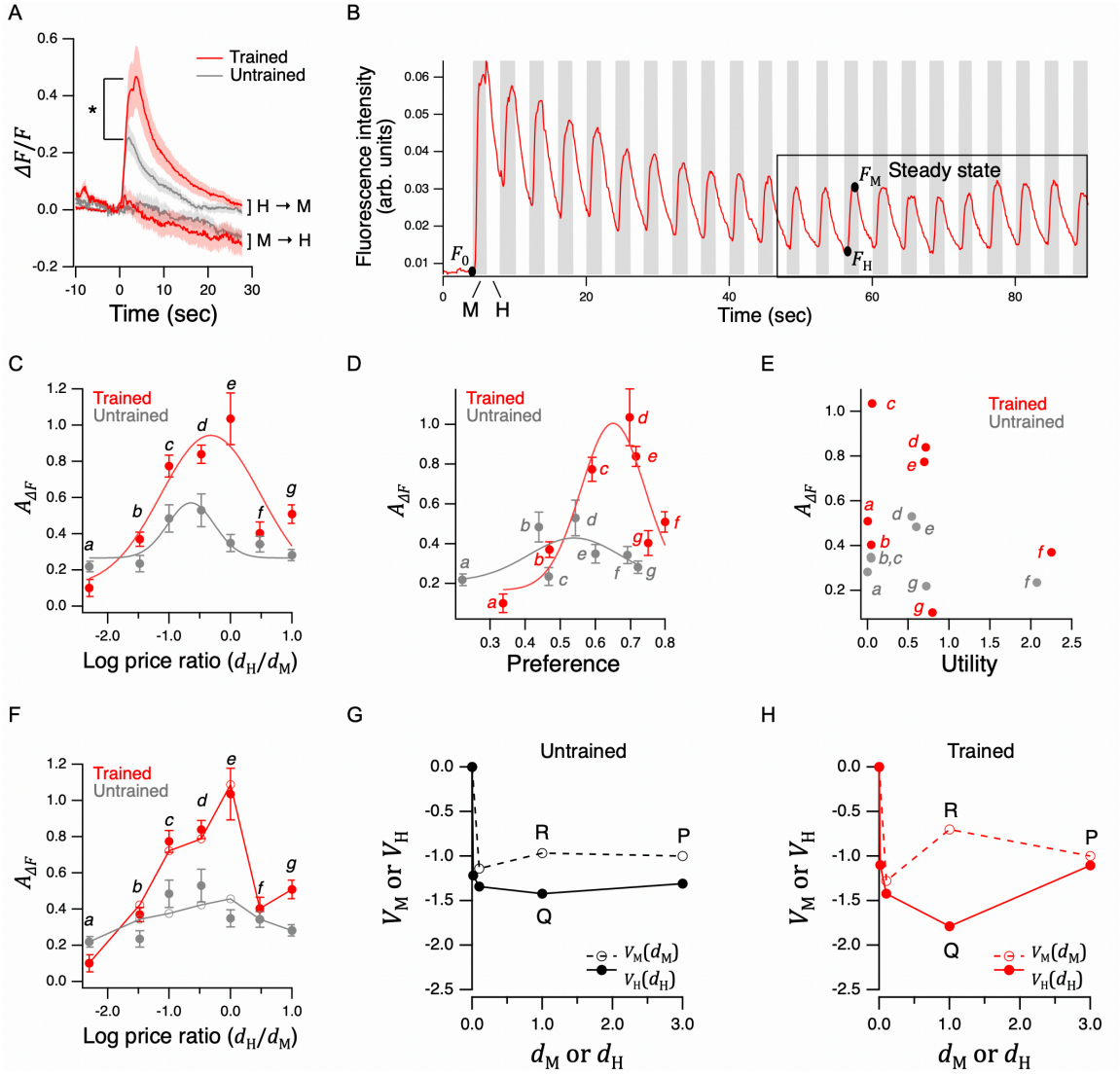

Figure 9. Characterization of AWC's response to bacteria foods in Y-chip assays.

A. Ensemble average of relative fluorescence versus time in response to transitions from H to M or M to H food. Both foods were presented at d = 1. Food was switched at t = 0. **B**. Typical fluorescence waveform in response to a series of transitions between H and M food. This stimulus approximates sensory input to the worm during a Y-chip experiment. Notation: F_0, basline fluoresence after sustained exposure to H food (≅ 2 min.); F_j, peak fluorescence following an H to M transition; F_i, trough fluorescence following an M to H transition. The box delineates the time period of presumptive steady-state behavior over which mean response amplitudes $A_{\Delta F}$ were computed for each recorded worm. **C-E**. Mean steady-state response amplitudes $A_{\Delta F}$ versus log price ratio, preference, and utility; the latter are fitted values in Fig. 6C,D. The quantity $A_{\Delta F}$ was averaged across worms within groups defined by training state (Trained vs. Untrained) and log price ratio (d_H/d_M) of presented foods The smooth curves are gaussian fits merely to illustrate the inverted U-shaped form of the data. *Italic letters*: points in Fig. 5B. **F**. Same as C, but with lines connecting points (open circles) indicating the response amplitudes predicted by the models of AWC shown in G and H. **G-H**. Relationship between AWC membrane hyperpolarization and density of H and M food in the AWC models for trained and untrained animals. Voltage units are arbitrary. These curves underlie the predicted response amplitudes shown in F. For example, the predicted value of mean $A_{\Delta F}$ at point *d* in E is computed as the voltage at P minus the voltage at Q. Similarly, $A_{\Delta F}$ at point *e* in E is computed as the voltage at R minus the voltage at Q. **A-E**. Shading and error bars ± SEM.

796

bends across the two food streams in the Y-chip, without the potentially confounding effects of changes in dwell time at different price ratios (Fig. 7B).

The imaging trace in Fig. 9B illustrates a typical fluorescence waveform in the experiment. AWC responded at two distinct time scales. On the longer time scale, it exhibited a positive transient that decayed over tens of seconds, reminiscent of the time course of responses to sustained changes from H to M food (Fig. 9A). On the shorter time scale, AWC responded with positive-going transients at each H→M transition, and negative-going transients at each M→H transition. The fact that positive transients occurred at the H→M transition, not the M→H transition, is consistent with AWC having a role in truncating head bends into the non-preferred food, as a means of biasing mean head angle toward the preferred side. The waveforms we obtained closely resemble the response to alternating presentations of plain buffer and buffer containing a food-related odor sensed by AWC (Kato *et al.*, 2013), suggesting the AWC perceives the transition to low food quality as similar to the transition to food-free medium.

Representational content of AWC's responses. To investigate AWC's role in utility maximization, we mapped its response function across the seven price ratios used in the GARP analysis of Fig. 5B,C. We assumed that the steady-state region of the imaging trace is a reasonably accurate representation of AWC activity during the 12 min. behavioral recordings in the Y-chip (Fig. 5B). We defined the amplitude of the calcium transients at steady-state as the mean fractional change in fluorescence between the peak at the end of an M step and its preceding trough at the end of an H step ($A_{\Delta F} = \langle (F_{\mathrm{M}} - F_{\mathrm{H}})/F_0 \rangle$). Reasoning that larger values of $A_{\Delta F}$ should correspond to stronger head-bend truncations, and thus greater head-position bias, we expected a monotonic, increasing relationship between $A_{\Delta F}$ and price ratio, consistent with the price-ratio curves of Fig. 5B. Additionally, $A_{\Delta F}$ should be approximately zero near the indifference point ($f_{\mathrm{H}} = 0.5$), and it should reverse sign when M is preferred over H ($f_{\mathrm{H}} < 0.5$). Contrary to expectations, AWC's response was an inverted U-shaped function for trained and untrained animals, non-zero near the indifference point, and did not reverse sign. Training greatly increased the height of the function's peak (Fig. 9C, effect of training, Supplemental Table 1[49]) and training appeared to cause a rightward shift in the position of the peak, toward higher price ratios. Similar curves were obtained when plotting $A_{\Delta F}$ against preference (Fig. 9D), whereas there was no obvious relationship between $A_{\Delta F}$ and utility, at least as inferred from the fitted utility values in Fig. 6C,D (Fig. 9E).

U-shaped neuronal response functions have been observed in primate orbitofrontal cortex in plots of mean firing rate against the ratio of offered amounts of two desirable juice rewards (Padoa-schioppa and Assad, 2006). However, regression of mean firing rate against “chosen value,” i.e., the value of the particular juice reward that was chosen, revealed an underlying linear relationship. For neurons having U-shaped response functions, chosen value was a far better predictor of neuronal responses than all other value-related quantities tested, including the offered value of each juice, total value of juice, difference in value between chosen and non-chosen juices, etc. We therefore considered whether AWC’s responses were linearly related to chosen value or related quantities.

It is straightforward to define relative food value and related quantities in terms of the densities of H and M food, together with the preference for each. For example, using the value of M food as the reference, the offered values of H and M at each price ratio in Fig. 5B for worms are given by

$$\begin{aligned} V_{\mathrm{M}} &= d_{\mathrm{M}} \\ V_{\mathrm{H}} &= w_{\mathrm{T}} d_{\mathrm{H}} \text{ or } w_{\mathrm{U}} d_{\mathrm{H}}, \end{aligned} \tag{13}$$

where w_{T} and w_{U} are, respectively, the ratio of food densities ($d_{\mathrm{M}}/d_{\mathrm{H}}$) at the indifference point ($f_{\mathrm{H}} = 0.5$) in trained and untrained animals, which can be computed by taking the inverse of r_0 in equation 7. The quantities w_{T} and w_{U} specify the number of units of M food that are equivalent to one unit of H food (assuming a linear valuation function in the vicinity of the indifference point). Alternatively, value can be equated with formal utility U, as inferred from fits of the CES utility function to the data in Fig. 6C,D. The resulting definitions of chosen value, chosen utility, and related quantities are given in Supplemental Table 2. To test whether AWC represents any of these quantities, we sought linear correlations between $A_{\Delta F}$ and each quantity, separately in trained and untrained animals. We found no significant correlations (Supplemental Table 3), making it unlikely that AWC represents the amount, value, or utility of food options in simple form.

Model of AWC function. Each of the functions in Supplemental Table 2 can be viewed as a unique economic model of the relationship between AWC activation ($A_{\Delta F}$) and food densities d_{M} and d_{H}. As none of these models fit our imaging data, we asked whether AWC's response function could explained by a biophysical model. We and others have noted that AWC's calcium signal falls in the presence of food (Fig. 8A), suggesting hyperpolarization. On the other hand, when food is removed or switched from H to M, AWC's calcium signal overshoots baseline, then recovers (Fig. 9A), suggesting transient depolarization. This response pattern is reminiscent of rebound excitation, a common property of a variety of neurons in other organisms (Huguenard and McCormick, 2007; Roberts, Li and Soffe, 2008; Kopp-Scheinpflug, Sinclair and Linden, 2018). In many cases, rebound excitation is triggered by a hyperpolarization activated inward current, I_{h}. An I_{h}–like current has been observed in excised patches from AWC (Nickell *et al.*, 2002). AWC expresses a number of ion channel subunit genes that could give rise to such currents. These include *chl-1* (Nehrke *et al.*, 2000), and *ocr-1*, a paralog of the TRPV homolog *osm-9* (Hoenderop *et al.*, 1999; Nilius *et al.*, 2000). AWC also expresses *egl-19* and *unc-2*, which encode subunits of voltage gated calcium channels. These, when triggered by rebound, could generate a calcium transient. Accordingly, we based the model on the assumption of rebound excitation in response to H→M transitions.

The model assumes that the magnitude of rebound is proportional to the change in membrane potential that occurs upon an H→M transition (reduced hyperpolarization), and that the height of the calcium transient is proportional to the magnitude of rebound. Formally, we modeled fluorescence changes as $A_{\Delta F} = k \cdot [V_{\mathrm{M}}(d_{\mathrm{M}}) - V_{\mathrm{H}}(d_{\mathrm{H}})]$, where V_{H} and V_{M} are functions relating d_{H} and d_{M} to membrane potential at the end of each presentation of H and the beginning of each presentation of M in an experiment such as Fig. 9B. For simplicity k, which has units of $A_{\Delta F}$/mV, was set to unity and membrane potential was represented in arbitrary units such that differences in V_{M} and V_{H} could be displayed directly on the $A_{\Delta F}$ axis in Fig. 9F. The model was fitted by an optimization routine (Brent's method for univariate functions (Press *et al.*, 2007)) that sought a mapping from the three different values of d_{M} and the four different values of d_{H} in Fig. 5B to a hypothetical value of membrane potential produced by these foods at each density; the model was fitted separately for trained and untrained animals. The only constraint on the fit was to minimize the discrepancy between modeled and actual values of $A_{\Delta F}$ at each price ratio. We made no assumptions as to the sign or form of the functions V_{M} and V_{H}, nor did we impose a smoothness constraint on these functions. We note that this optimization problem is non-trivial, as most optical densities of H and M food appear in multiple price ratios, thereby reducing the number of degrees of freedom in the model. For example, d_{M} = 3 at points *a*, *b* and *d* in Fig. 5B, so V_{M} is must be the same for each of these points; similarly, d_{H} = 1 at points *d*, *e*, and *g*, so V_{H} must be the same at these points also.

Despite the model's simplicity, we obtained remarkably good fits to the imaging data (Fig. 9F). The model explains 98.5% of the variance in trained animals. It accurately reproduces large scale trends, such as the overall non-monotonicity of the relationship between $A_{\Delta F}$ and log price ratio. It also reproduces small scale trends including, for example, the difference in $A_{\Delta F}$ at points *f* and *g*. In the case of untrained animals, the model explains 53.6% of the variance. It reproduced the large-scale non-monotonicity in the data, but did not in general recapitulate small-scale trends. This may reflect the fact that in the absence of food quality training, AWC responses are somewhat weaker and more variable. A satisfying aspect of the model is that V_{M} and V_{H} are biologically plausible functions of food density (Fig. 9G,H). The functions for untrained animals can be thought of as a hyperpolarizing response that saturates as food density increases. The functions in trained animals can be viewed similarly, except for having exaggerated deviations from each other at $d_{\mathrm{H}} = d_{\mathrm{M}} = 1$. These functions are testable predictions of the model.

Finally, the shapes of V_{M} and V_{H} funcfions suggest a novel role for AWC that is distinct from representing value or utility. In untrained animals, the effect of food quality on membrane potential is modest relative to the effect of the overall amount of food, suggesting that the baseline role of AWC is mainly to report food quantity. In trained animals, however, the neuron becomes tuned for situations in which H and M food are at similar densities ($\log(d_{\mathrm{H}}/d_{\mathrm{M}}) \cong 0$), where discriminating foods of different quality, now regardless of price, becomes important for being able to consume more of the better option.

Discussion

There is growing evidence that *C. elegans* behaves as if capable of several forms of valuation including those inherent in cost-benefit decisions, transitivity of binary preferences, and independence of irrelevant alternatives (Barrios, Nurrish and Emmons, 2008; Bendesky *et al.*, 2011; Shinkai, Yamamoto, Fujiwara, Tabata, Murayama, Hirotsu, Daisuke D. Ikeda, *et al.*, 2011; Ghosh *et al.*, 2016; Cohen *et al.*, 2019; Iwanir *et al.*, 2019). The present work breaks new ground in the study of valuation in this simple organism in four key respects. (1) *C. elegans* food choices obey the classic law of supply and demand (Fig. 5A). This law has been shown to apply not just to humans but to a variety of model organisms (Kagel *et al.*, 1975; W K Bickel, L Green, 1995)(Kagel, Battalio and Green, 1995), but none as simple as *C. elegans*. (2) *C. elegans* behaves exactly as if maximizing utility (Fig. 5C). When challenged with multiple trade-offs between food quality and price, its choices satisfy the necessary and sufficient conditions for utility maximization. An organism that maximizes utility also maximizes subjective value, for it is reasonable to maximize only that which is valued. To our knowledge this is the first demonstration of value-based decision making according to GARP in an invertebrate (Fig. 5C). (3) *C. elegans* food-consumption decisions are well fit by the CES utility function (Fig. 6C,D). This function is widely used to model human consumers, but the extent to which it applies to infra-human species remains an open question (Fréchette, 2016). Here we show that the CES function accurately models consumption decisions in an organism that diverged from humans 600 million years ago (Raible and Arendt, 2004) (Fig. 6C,D), which provides new evidence of the function's universality. (4) In addition to demonstrating utility maximization in *C. elegans*, we have outlined a plausible mechanism for it. The *C. elegans* price-ratio curve is monotonic-increasing (Fig. 5B), a property that literally guarantees adherence to GARP, as discussed below (Fig. 10). Importantly, such a price-ratio curve is simple to implement at the neuronal level, requiring only that chemosensory neurons can modulate the amplitude of ongoing locomotory head-bends monotonically in response to differences in food value on either side of the body.

The main limitation of the present study is high probability of a false positive finding of utility maximization in Fig. 5C. One contributing factor to this problem is the comparatively small number of budget lines in our budget ensemble, attributable to the time consuming nature of single-worm experiments with large sample sizes. Another factor is the somewhat uneven coverage of choice space, with two budget lines close to the y axis (*a* and *b*). We included these budget lines to make a stronger case for complex decision making in the worm by demonstrating preference reversals (Fig. 5B); unfortunately, this required presenting H food at very low density. We were able to address this limitation by showing that the price-ratio curve of Fig. 5B predicted the absence of transitivity violations in a larger, more stringent budget ensemble (Fig. 5D). Moreover, we show below that the absence of violations in the larger ensemble is essentially guaranteed by the monotonic form of the worm's price-ratio curve.

Distinctions between GARP and binary transitivity

Assessment of utility maximization by GARP involves demonstration of internally consistent preferences. This means non-violation of transitivity relationships inherent in directly revealed preferences, as well as those revealed indirectly through sequences of directly revealed preferences. The scientific literature on transitive choice in animals is extensive, encompassing a wide range of vertebrates: primates (Addessi *et al.*, 2008), birds (Mazur and Coe, 1987; Sumpter, Temple and Foster, 1999; Schuck-Paim and Kacelnik, 2002), and fish (Dechaume-Moncharmont *et al.*, 2013). Many invertebrates also exhibit transitivity: bees (Shafir, 1994), fruit flies (Arbuthnott *et al.*, 2017), nematodes (Cohen *et al.*, 2019; Iwanir *et al.*, 2019), and even slime molds (Latty and Beekman, 2011). However, these studies have focused almost entirely on binary transitivity, meaning either-or decisions between pairs of unitary items. Transitivity in this sense can be impressive, even in simple organisms. Choices of male fruit flies presented with pairs of genetically distinct females drawn from 10 divergent inbred strains form an inviolate transitive hierarchy of order 10 (Arbuthnott *et al.*, 2017). Striking examples notwithstanding, binary transitivity is not a sufficient condition for utility maximization. That is because in binary choices there is no notion of amount. It is therefore impossible to assess whether choices are consistent with the rule "more is better" which, as illustrated in Fig. 1A, is a necessary condition for utility maximization. Here we have demonstrated a form of transitivity in which not only the quality of goods but also their offered amount (hence price) is taken into account by the
.

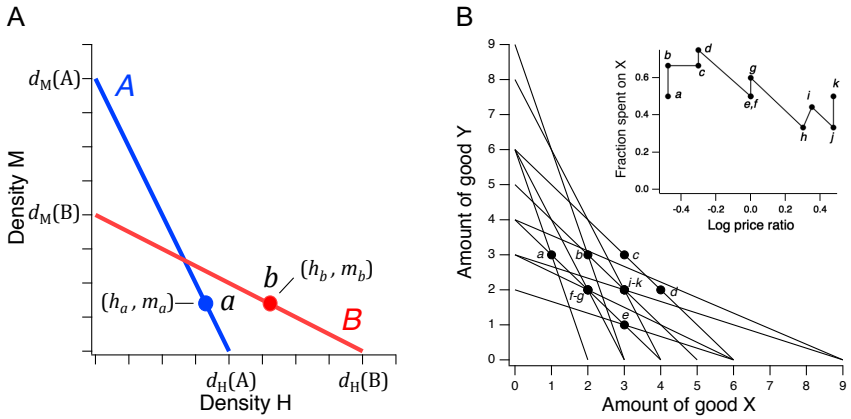

962
963
964 **Figure 10. Price ratio curves and utility maximization**
965
966 **A**. A pair of intersecting budget lines wherein choices *a* and *b* are governed by price ratio curve (not shown)
967 that is monotonic-increasing. To support a direct utility violation, *a* must be inside the triangle formed by *B*,
968 and *b* must be inside the triangle formed by *A*. However, by monotonicity, *b* must lie to the right of *a*, for
969 reasons described in the text. Thus, b cannot lie inside of triangle *A*, preventing a direct violation. **B**. Choice
970 data from a human participant in a GARP experiment (Camille *et al.*, 2011). The data are consistent with
971 utility maximization. *Inset*, price ratio data inferred from the experiment. Log price ratios for points *a*-*k* are
972 calculated as $log\, X_z/Y_z$, where X_z and Y_z are, respectively, the x and y intercepts of budget line z. The frac-
973 tion of total budget spent on good X is computed as x_z/X_z, where x_z is the amount of good X chosen on
974 line z.
975

organism. The full set of transitivity relationships exhibited by worms in our study is illustrated in Supplemental Fig. 3

What is being maximized?

Utility maximization raises the ineluctable question of what is being maximized. At this point, however, it is easier to identify what is *not* being maximized. Three ethologically plausible maximization strategies can be ruled out by simple inspection of Fig. 5C. The worm is clearly not maximizing the amount of high quality food consumed, as that would have resulted in corner solutions such as those illustrated in Fig. 6B. Nor is the worm maximizing the overall amount of food consumed. That would have resulted in feeding exclusively in whichever of the two streams carried denser food, yielding corner solutions at the highest density on each budget line (except at point *e*, where densities are equal and so the worm would be indifferent, whereas it actually preferred H food). Finally, and perhaps surprisingly, the worm is probably not maximizing its potential for rapid growth, at least in terms of a simple model in which growth rate of an individual (the inverse of the number of days to grow from hatchling to day 1 adult) is proportional to the weighted sum of the amounts of H and M food eaten, where the weighting factors are the observed growth rates in each food type. This model fails to explain our data because growth rates in H and M food are quite similar: 0.49 and 0.42 $days^{-1}$ for H and M food, respectively (Avery and Shtonda, 2003). Such a model therefore predicts an outcome similar to maximizing amount of food consumed (except at point *e*, where now H food would be favored).

The worm's preference for non-corner solutions, called "interior solutions," is consistent with at least two hypotheses concerning what *is* being maximized. Perhaps the worm is maximizing something having to do with mixtures of the two foods, reminiscent of "a taste for variety" in economics (Senior, 1836; Jevons, 1871). This would be an appropriate strategy if, for example, the two foods had unique essential nutrients, but we currently have no evidence for or against this. A second hypothesis is that interior solutions arise because the worm is balancing the benefit of consuming the better food option against the cost of forgoing the possibility of the sudden appearance of an even better option on the other side; this hypothesis mirrors an exploitation-exploration trade-off. Alternatively, neuro-mechanical constraints such as chemosensory transduction delays coupled with behavioral momentum (difficulty of instantaneously reversing the current head bend), could be a factor in producing interior solutions. Further work is needed to resolve this issue.

Establishment of subjective value assignments

That learning alters food preferences in *C. elegans* is well established (Ardiel and Rankin, 2010). We extended these findings by showing that worms are capable of explicit food quality learning for palatable foods at least as late as larval stage L4 (Fig. 2). We also found evidence for latent acquisition of food preferences in that untrained worms encountering H and M food for the first time strongly preferred H food. The fact that this effect requires intact dopamine signaling (Fig. 2D) suggests it too may be a form of learning.

Explicit and latent food quality learning may be dissociable in that the former, but not the latter, exhibits a requirement for the homeobox gene *ceh-36* (Fig. 2B). In one simple model, AWC, ASE, or both neurons are loci of explicit food memories, whereas some or all of the other chemosensory neurons mediate latent learning. In partial support of this model, AWC's response to either removal of H food (Fig. 8C), or H→M transitions (Fig. 9A,C), is strongly enhanced by explicit training. It will now be important to determine whether food responses in ASE neurons are also modified by explicit training, and whether the responses of other chemosensory neurons are modified mainly by latent learning.

The fact that in *cat-2* mutants latent and explicit learning were reduced in trained and untrained worms (Fig. 2D) implicates dopamine signaling in the acquisition or expression of food quality memories. One attractive hypothesis is that during training, dopamine neuron activity in *C. elegans* signals reward, as it does in many other organisms. In support of this model, *cat-2* is required for learned associations between salt cues and drugs of abuse that co-opt the reward systems, such as cocaine and methamphetamine (Musselman *et al.*, 2012) as well acquisition of alcohol preference (Lee, Jee and McIntire, 2009). Similarly, the *C. elegans*

gene *asic-1*, a member of the degenerin/epithelial sodium channel family that is mainly expressed at pre-synaptic terminals of dopaminergic neurons, is required for learned associations between tastes or odors and the presence of food (Voglis and Tavernarakis, 2008).

Monotonic-increasing price-ratio curves guarantee adherence to GARP

The price-ratio data in Fig. 5B are well fit by smooth curves that are monotonic-increasing (strictly, *non-decreasing*; equation 7). Here we offer a proof that a monotonic-increasing price-ratio curve precludes utility violations. In Fig. 10A, budget line *A* has the steeper slope of the two lines. Point a represents any location on *A* such that $b \succ a$ could be revealed directly (meaning a is between the *A*-*B* intersection and the x axis; see Fig. 1A). Point b, on the other hand, represents any location on *B* that is consistent with monotonicity, conditioned on the location of a. As the slope of *B* is shallower than the slope of *A*, and price ratio $r = d_{\mathrm{H}}/d_{\mathrm{M}}$, *B* has the greater price ratio. Thus $r_{\mathrm{B}} > r_{\mathrm{A}}$, and so by monotonicity, $f_{\mathrm{H}}(r_B) > f_{\mathrm{H}}(r_A)$. Furthermore, by construction $d_{\mathrm{H}}(B) > d_{\mathrm{H}}(A)$. Finally, by equation 5, the x coordinates of a and b are $h_a = f_{\mathrm{H}}(r_A) \cdot d_{\mathrm{H}}(A)$ and $h_b = f_{\mathrm{H}}(r_B) \cdot d_{\mathrm{H}}(B)$, respectively. Given these inequalities, $h_b > h_a$, and point b must always lie to the right of a. This means b will always be preferred to a; it can never be revealed that $a \succ b$. Monotonicity thereby precludes direct violations and, as direct violations are necessary for indirect violations (Rose, 1958; Heufer, 2009), the latter are also precluded. Thus, monotonic price-ratio curves guarantee adherence to GARP. This logic explains our finding that when modeling *C. elegans* food choice by the worm's price-ratio curve, the probability of finding utility maximization in the 11-budget ensemble was ≥ 0.98 (the exceptions being due to sampling noise). Although monotonic-increasing price-ratio curves guarantee utility maximization, they are not necessary for it. Fig. 10B shows data from a human subject who exhibits no utility violations, yet whose price-ratio curve is clearly non-monotonic. Thus, in relying upon monotonic price-ratio curves, the worm's choice strategy may be an adaptation for rational consumption behavior under the constraint of limited computational capacity.

A neuronal mechanism of utility maximization

The following simple model suggests how a monotonic price-ratio curve, and thus utility maximization, could be achieved by the *C. elegans* klinotaxis circuit. The food-sensitive chemosensory off-cells (AWC, ASER, AWB, ASH, ASK) and on-cells (ASEL, AFD, AWA, ASJ, BAG, ASI, ADF) activate, respectively, when the cell's preferred stimulus is removed or delivered (Zaslaver *et al.*, 2015). The off-cells AWC and ASER are known to truncate head bends when exogenously activated (Kocabas *et al.*, 2012). The model assumes that other off-cells do likewise, whereas on-cells extend head bends. Provided that summed activations of all off-cells and on-cells are, respectively, monotonic functions of price ratio, the amplitude of head-bend truncations and extensions will also be monotonic with respect to price ratio. Given the sinusoidal kinematics of *C. elegans* locomotion, this relationship necessarily extends to relative dwell time on the side of the preferred food option, thereby increasing the fraction of pumps on that side. The non-monotonic activation function of AWC (Fig. 9) could be compensated by activations of other chemosensory neurons at price ratios greater than unity. This model can now be tested by recording and stimulating neurons in the klinotaxis circuit during choices of the type studied here.

Conclusion

All animals forage so as to obtain sufficient food at minimal cost. Omnivores like humans, *C. elegans*, and other species, face the additional challenge of reconciling trade-offs between food quality and a wide variety of costs, such as energy, time (lost opportunity), and risk. Our findings expand the scope of comparative studies already in progress in ethology, behavioral ecology, and neuroeconomics to probe the limits of classical economic theory in explaining such fundamental trade-offs (Kalenscher, Wingerden and Hayden, 2011; Pearson, Watson and Platt, 2014). Is the classical theory universally applicable to animal behavior? To what extent can it be grounded in neurophysiology? The small size and unequalled annotation of the *C. elegans* nervous system (White JG, Southgate E, Thomson JN, 1986; Jarrell *et al.*, 2012; Hammarlund *et al.*, 2018; Cook *et al.*, 2019; Brittin *et al.*, 2021; Hobert, 2021), coupled with recent advances in brain wide imaging in this organism (Kato *et al.*, 2015; Nguyen *et al.*, 2016; Venkatachalam *et al.*, 2016) offer unique advantages in answering these questions.

MATERIALS AND METHODS

Worm strains. The following genotypes were used:

Experiment	Figure	Genotype
Wild type decision making	2, 4-9	N2
Requirement for AWC/ASE neurons	2B, 7D	*ceh-36(ky646)*
Requirement for dopamine signaling	2D	*cat-2(tm2261)*
Calcium imaging from AWC neurons	9	ntIs1703[str-2::GCamp6s-wcherry; unc-122::dsred2]
Proportion of time on food	2 (suppl.)	*cat-2(n4547), cat-2(e1112)*

Bacteria strains. Streptomycin resistant strains of three species were used: *E. coli* (OP50 DA 837) representing standard laboratory food, *Comamonas* sp. (DA1877) representing high quality food (H), and *Bacillus simplex* (DA1885), representing medium quality food (M). To culture bacteria, a small scraping of frozen stock was transferred to 400 mL of LB broth in a 500 mL flask to which streptomycin (50 µg/mL) added to inhibit competitive bacterial growth. Cultures were grown overnight in on a shaker (3 Hz) at 35 C. Optical density (OD) of bacteria suspensions was measured at 600 nm.

Worm cultivation and training. Worms were synchronized by isolating eggs from 10 gravid adults allowed to lay eggs for five hours. Progeny were cultivated until late larval stage L3 at 20 ˚C on 50 cm plates containing low-density nematode growth medium (NGM; (Brenner, 1974)) seeded with standard laboratory food (*E. coli* OP50). In experiments involving *explicit food quality training*, worms were washed three times in M9 buffer, pelleted by sedimentation, then transferred in a 2 µL aliquot (~150 worms) to a training plate (50 mm diam.) filled with bactopeptone-free NGM containing 200 µg/mL streptomycin. Training plates were prepared one day in advance by spotting them with eight patches each of H and M food. Patches were formed by pipetting 10 µL aliquots of bacteria culture, suspended in LB broth at OD = 10, in a 4 × 4 grid with 10 mm between patch centers (Fig. 2A). Control plates were spotted with patches of OP50 in the same pattern. Worms resided on training plates for 18-24 hours before testing. In experiments involving the *food familiarity effect*, training plates contained 16 patches of either H or M food prepared in the same way.

Accumulation assays. In *open-field assays*, NGM test plates (50 mm diameter) were spotted with one patch each of H and M food (100 µL, OD = 10) separated by 25 mm. In *T-maze assays*, a mask formed by laser cutting 2 mm thick ethylene-vinyl acetate foam sheets (Supplemental Fig. 1; Supplemental Table 4. The mask was placed on the NGM surface and baited with the same amounts of H and M food. After training, worms were washed and transferred as above to the plate center or the starting point in the T-maze. Preference at each time point was computed as $(N_{\mathrm{H}} - N_{\mathrm{M}})/(N_{\mathrm{H}} + N_{\mathrm{M}})$, where N is the number of worms in contact with the food-type indicated by the subscript. Worms were counted by eye with the aid of a tally counter; the experimenter was blind to condition.

Food dwell-time assays. Dwell-time on food patches was measured as described previously (Cermak *et al.*, 2020). Assay plates were standard 10 cm diameter petri dishes filled with low-peptone (0.2 g/L) nematode growth medium, seeded with 200 mL *E. coli* OP50. Low-peptone medium ensured thin bacterial lawns for improved tracking optics. Roughly circular lawns were created with a spreader, and plates were left to dry overnight before use. For recordings, a single 72 hr old adult animal was picked to an assay plate, allowed to accommodate for 10 min, and then tracked for approximately six hours at 20 fps using the described automated tracking microscope. Prior to tracking, the lawn boundary was annotated by manually circumscribing it with the microscope. This procedure enabled post-hoc determination of when the worm was on or off the lawn.

System for recording food choice in semi-restrained worms. The system comprised (1) a food delivery system, (2) instrumentation for electrophysiological recording, and (3) a video camera for recording behavior (Fig. 3).

(1) Food delivery system. Bacteria suspensions, and bacteria-free buffer, were held in 20 mL reservoirs (syringes with plungers removed) fitted with stopcocks. Reservoirs were suspended 50 cm above the chip and connected to it via polyethylene tubing (PE-9) fitted with 1.5 mm diameter × 12.5 mm stainless steel nipples (17 Ga, × 0.500", New England Small Tube, Litchfield, New Hampshire). To minimize settling of bacteria, a miniature magnetic stir bar in each reservoir was agitated periodically during experiments by moving a small hand-held magnet. The layout of the Y-chip was similar in all main respects to a previous design (McCormick *et al.*, 2011); feature height was 55 µm. Flow rate in the chip was regulated by a peristaltic pump (model 426-2000, Labconco, Kansas City, MO, USA) attached to chip's outlet port.

(2) Electrophysiology. Electropharyngeograms were recorded by means of electrodes (stainless steel nipples, see above) inserted into the worm port and fluid outlet. In this configuration they were used to measure the voltage differences that occur between the worm's head and tail during pharyngeal muscle action potentials. The vacuum clamp accentuates these voltage differences by increasing the electrical resistance between head and tail. Voltage differences between electrodes were amplified by a differential amplifier (model 1700, AM Systems, Sequim, Washington) and digitized (2 kHz) for later analysis (USB-9215A, National Instruments, Austin, Texas). Digitized recordings were bandpass filtered between 5 and 200 Hz. E and R spikes were detected offline by a manually adjusted threshold in custom data analysis software. Instantaneous pumping rate was computed using a 5 sec. sliding window average (forward looking).

(3) Videography. The worm was imaged using a stereomicroscope (Wild M3C, Leica, Buffalo Grove, Illinois) with a 1.5× objective, and a video camera (VE-CCDTX, DATG MTI, Michigan City, Illinois) with a frame rate of 30 Hz. Individual frames were analyzed by MATLAB scripts (Mathworks, Natick, MA) to extract head angle of the worm as previously described (McCormick et al. 2011). First, each frame was thresholded to identify the worm's head and neck region, which was then skeletonized to obtain its centerline (white line, Fig. 3B) and head angle (θ) was defined as described Fig. 3B. Values of head angle when the worm was exhibiting presumptive reversal behavior (Faumont and Lockery, 2006) where excluded manually, without knowledge of experimental condition.

Single-worm food choice assays. To minimize extraneous olfactory or gustatory cues, washed bacteria were resuspended in a minimal buffer to the desired OD; the buffer contained (in mM): 1 $MgSO_4$, 10 HEPES adjusted 350-360 mOsm (glycerol). We found that OD = 1 respectively corresponds to approximately 2.35 × 10^9 and 2.00 × 10^9 colony forming units/mL of *Comamonas* and *Simplex*, respectively. However, OD is a better proxy for mass of bacteria in a suspended sample (Koch, 1970; Stevenson *et al.*, 2016). After training, worms were washed and transferred to foodless plates for 1-2 hours of food deprivation. At the start of the assay, the Y-chip was filled with buffer solution and a worm was inserted into the chip by liquid transfer using a syringe fitting with PE tubing and a steel nipple. During a 2 min. accommodation period, both streams carried buffer and the video and electrophysiological recordings were initiated. After accommodation, both streams were switched to particular food types according to the needs of the experiment. In *food-familiarity* (Fig. 4A) and *food-density* experiments (Fig. 4C-D) channels 1 and 4 carried the same food (H or M). In *food quality learning* (Fig. 4B) and *integration of preference and price* (Fig. 5B), channel 1 carried H food and channel 4 carried M food at optical densities given in the legends or indicated in the figures. Feeding was recorded for 12 min. after food onset. Mean pumping frequency was computed as the number of pumps (paired E and R spikes) divided by total observation time. Preference (f_{H}) was defined as the fraction of pumps emitted when the tip of the worm's head, where the mouth is located, was in H food, as detected in the synchronized video recording. Specifically, $f_{\mathrm{H}} = N_{\mathrm{H}}/(N_{\mathrm{H}} + N_{\mathrm{M}})$, where N_{H} and N_{M} are the number of pumps in H and M food, respectively; on this scale, $f_{\mathrm{H}} = 0.5$ constitutes equal preference for the two foods or, in economic terms, indifference between the two options.

Fitting utility functions to preference data

To fit the CES function (equation 9) to the choice data in Fig. 6C,D, we estimated the parameters β and ρ using two-limit tobit maximum likelihood. Values of the error term were drawn from identical and independent normal distributions (Andreoni and Miller, 2002).

System for calcium imaging of neuronal activity

For recording from AWC neurons, the genetically encoded calcium indicator GCaMP6s was expressed under control of the *str-2* promoter. Late L4 or early adult worms were immobilized in a newly designed microfluidic imaging chip (Supplemental Fig. 4) based on a previous device in which the worm's nose protrudes into a switchable stimulus stream (Chronis et al., 2007). Chip feature-height was 30 µm. The chip was adapted for rapid switching. The switching time constant in a microfluidic chip that is driven by a constant current source (e.g., a syringe pump) is equal to the product of the system's compliance (C) and fluidic resistance of the chip (R). To reduce compliance we used rigid inlet tubing and to reduce resistance fabricated wide channels.

To improve stimulus stability, fluid flow was driven by a syringe pump rather than gravity or pressure. Two of the four syringes in the pump were filled with H food and two with M food. Syringes were connected to the chip such that if all four channels were flowing into the chip, the cross-sectional flow at the point of confluence near the worm would be H_2 H_1 M_1 M_2. Stimulus presentation was automated utilizing a microprocessor to control a pair of two-way solenoid valves (LFAA1201610H, The Lee Company, Westbrook, Connecticut) in series with the syringes H_1 and M_1; the outer channels H_2 and M_2 flowed continuously. To present H food, the stimulus pattern was H_2 H_1 M_1; to present M food the pattern was H_1 M_1 M_2. As all channels flowed at the same rate, each occupied 1/3 of the cross-sectional flow at the worm's position with the result that small fluctuations in the position of fluidic interfaces were kept far from the worm's nose.

A Hamamatsu CCD camera (model C11254) controlled by HCImage was used to capture stacks of TIFF images at 10 frames/sec. Images were analyzed by manually drawing a region of interest (ROI) comprising a tightly cropped segment of the neurite connecting the cilium and soma. Mean background fluorescence was estimated from a 2-pixel thick margin situated 2 pixels outside the ROI in each frame. Absolute neuronal fluorescence was quantified as the mean of the 200 brightest pixels in the ROI, minus mean background. Finally, fluorescence values were expressed as fractional change relative to pre-stimulus baseline absolute fluorescence. Traces shown were not bleach-corrected.

Microfabrication. Devices were fabricated using standard soft lithography (Xia and Whitesides, 1998; Xia *et al.*, 2008). Silicon-wafer masters were created by exposing a layer of SU-8 2025 resist (Microchem, Newton, MA) through a transparency mask and developing the master in a bath of glycol monomethyl ether acetate (PGMEA). CAD files for the Y-chip and the imaging chip are provided in Supplemental Table 4. Masters were treated with tridecafluoro-1,1,2,2-tetrahydrooctyl trichlorosilane (Gelest, Morrisville, Pennsylvania) vapor to facilitate release. Devices were formed by casting polydimethylsiloxane pre-polymer (PDMS Sylgard 184, Dow Corning, Corning, NY) against masters. After curing and mold release, holes for external connections (fluidic inlets and outlets, worm injection, and electrodes) were formed using a 1.5 diameter punch. Devices were exposed to an air plasma then bonded to glass slides (Y-chip) or coverslips (calcium imaging chip).

Statistics. The following statistical tests were employed according to experimental design: *t*-test, two-factor analysis of variance, 2-factor analysis of variance with repeated measures on one factor. Statistical details (comparison, statistical test, degrees of freedom, *p* value) are compiled in Supplemental Table 1, and referred to in the text by the notation Supplemental Table 1^n, where *n* is the row number.

ACKNOWLEDGEMENTS

This research was supported by MH051383 and GM129576 from the National Institutes of Health (SRL). We thank Mei Zhen for the GCaMP-6s::wCherry probe used in imaging experiments, Jonathan Millet for assistance, and Anastasia Levichev for comments on the manuscript.

COMPETING INTERESTS

S.R.L. is co-founder and Chief Technology Officer of InVivo Biosystems, Inc., which manufactures instrumentation for recording electropharyngeograms. The other authors have no competing interests.

REFERENCES

Addessi, E. *et al.* (2008) 'Preference Transitivity and Symbolic Representation in Capuchin Monkeys (Cebus apella)', *PLoS ONE*, 3(6), pp. 4–11. doi: 10.1371/journal.pone.0002414.

Afriat, S. N. (1967) 'The Construction of Utility Functions from Expenditure Data', *International Economic Review*. JSTOR, 8(1), pp. 67–77. doi: 10.2307/2525382.

Andreoni, J. and Miller, J. (2002) 'Giving According To Garp', *Econometrica*, 70(2), pp. 737–753. Available at: http://www.jstor.org/stable/2692289.

Arbuthnott, D. *et al.* (2017) 'Mate choice in fruit flies is rational and adaptive', *Nature Comm*, (May 2016). doi: 10.1038/ncomms13953.

Ardiel, E. L. and Rankin, C. H. (2010) 'An elegant mind: Learning and memory in Caenorhabditis elegans', *Learning and Memory*, pp. 191–201. doi: 10.1101/lm.960510.

Avery, L. and Horvitz, H. R. (1990) 'Effects of starvation and neuroactive drugs on', *Journal of Experimental Zoology*. J Exp Zool, 253(3), pp. 263–270. doi: 10.1002/jez.1402530305.

Avery, L. and Shtonda, B. B. (2003) 'Food transport in the C. elegans pharynx', *Journal of Experimental Biology*. doi: 10.1242/jeb.00433.

Barrios, A., Nurrish, S. and Emmons, S. W. (2008) 'Sensory Regulation of C. elegans Male Mate-Searching Behavior', *Current Biology*. Elsevier Ltd, 18(23), pp. 1865–1871. doi: 10.1016/j.cub.2008.10.050.

Bendesky, A. *et al.* (2011) 'Catecholamine receptor polymorphisms affect decision-making in C . elegans', *Nature*. Nature Publishing Group. doi: 10.1038/nature09821.

Brenner, S. (1974) 'The genetics of Caenorhabditis elegans', *Genetics*, 77, pp. 71–94.

Brittin, C. A. *et al.* (2021) 'A multi-scale brain map derived from whole-brain volumetric reconstructions', *Nature*. Nature Research, 591(7848), pp. 105–110. doi: 10.1038/s41586-021-03284-x.

Burghart, D. R., Glimcher, P. W. and Lazzaro, S. . (2013) 'An expected utility maximizer walks into a bar...', *Journal of Risk and Uncertainty*, 46, pp. 215–246.

Busch, K. E. and Olofsson, B. (2012) 'Should I stay or should I go?', *Worm*, 1(3), pp. 1–5.

Calvo, A. C. *et al.* (2011) 'Divergence in enzyme regulation between Caenorhabditis elegans and human tyrosine hydroxylase , the key enzyme in the synthesis of dopamine', *Biochemical Journal*, 141, pp. 133–141. doi: 10.1042/BJ20101561.

Camille, N. *et al.* (2011) 'Ventromedial frontal lobe damage disrupts value maximization in humans', *Journal of Neuroscience*. doi: 10.1523/JNEUROSCI.6527-10.2011.

Cermak, N. *et al.* (2020) 'Whole-organism behavioral profiling reveals a role for dopamine in statedependent motor program coupling in C. Elegans', *eLife*, 9, pp. 1–34. doi: 10.7554/eLife.57093.

Chalasani, S. H. *et al.* (2007) 'Dissecting a circuit for olfactory behaviour in Caenorhabditis elegans', *Nature*, 450(November), pp. 63–70. doi: 10.1038/nature06292.

Chalfie, M. *et al.* (1985) 'The neural circuit for touch sensitivity in Caenorhabditis elegans', *Journal of Neuroscience*, 5(4), pp. 956–964. doi: 10.1523/jneurosci.05-04-00956.1985.

Choi, J. I. *et al.* (2016) 'A natural odor attraction between lactic acid bacteria and the nematode Caenorhabditis elegans', *ISME Journal*. Nature Publishing Group, 10(3), pp. 558–567. doi: 10.1038/ismej.2015.134.

Chung, H.-K., Tymula, A. and Glimcher, P. (2017) 'The Reduction of Ventrolateral Prefrontal Cortex Gray Matter Volume Correlates with Loss of Economic Rationality in Aging'. doi: 10.1523/JNEUROSCI.1171-17.2017.

Cohen, D. *et al.* (2019) 'Bounded rationality in C. elegans is explained by circuit-specific normalization in chemosensory pathways', *Nature Communications*. Springer US, 10(1), pp. 1–12. doi: 10.1038/s41467-019-11715-7.

Colbert, H. A. and Bargmann, C. I. (1995) 'Odorant-specific adaptation pathways generate olfactory plasticity in C. elegans', *Neuron*. doi: 10.1016/0896-6273(95)90224-4.

Cook, S. J. *et al.* (2019) 'Whole-animal connectomes of both Caenorhabditis elegans sexes', *Nature*. Springer US, 571(7763), pp. 63–71. doi: 10.1038/s41586-019-1352-7.

Culotti, J. and Russell, R. (1978) 'Osmotic avoidance defective mutants of the nematode C. elegans', *Genetics*, 90, pp. 243–256.

Dechaume-Moncharmont, F.-X. *et al.* (2013) 'Female mate choice in convict cichlids is transitive and consistent with a self-referent directional preference', *Frontiers in Zoology*, 10, pp. 1–10. Available at: http://www.frontiersinzoology.com/content/10/1/69.

Fang-yen, C., Avery, L. and Samuel, A. D. T. (2009) 'Two size-selective mechanisms specifically trap bacteria-sized food particles in Caenorhabditis elegans', *Proceedings of the National Academy of Sciences of the United States of America*, 106(47), pp. 1–4.
Faumont, S., Lindsay, T. H. and Lockery, S. R. (2012) 'Neuronal microcircuits for decision making in C. elegans', *Current Opinion in Neurobiology*, pp. 580–591. doi: 10.1016/j.conb.2012.05.005.
Faumont, S. and Lockery, S. R. (2006) 'The awake behaving worm: Simultaneous imaging of neuronal activity and behavior in intact animals at millimeter scale', *Journal of Neurophysiology*, 95(3). doi: 10.1152/jn.01050.2005.
Fréchette, G. R. (2016) 'Experimental economics across subject populations', in Kagel, J. H. and Roth, A. E. (eds) *The Handbook of Experimental Economics*. Princeton: Princeton Universitiy Press, pp. 000–000.
Frezal, L. and Felix, M.-A. (2015) 'C . elegans outside the Petri dish', *eLife*, pp. 1–14. doi: 10.7554/eLife.05849.
Ghosh, D. D. *et al.* (2016) 'Neural Architecture of Hunger-Dependent Multisensory Decision Making in C. elegans', *Neuron*. Elsevier Inc., 92(5), pp. 1049–1062. doi: 10.1016/j.neuron.2016.10.030.
Gordus A, Pokala N, Levy S, Flavell SW, B. C. (2015) 'Feedback from network states generates variability in a probabilistic olfactory circuit', *Cell*, 161, pp. 215–227. d.
Ha, H. *et al.* (2010) 'Article Functional Organization of a Neural Network for Aversive Olfactory Learning in Caenorhabditis elegans', *Neuron*, 68, pp. 1173–1186. doi: 10.1016/j.neuron.2010.11.025.
Hammarlund, M. *et al.* (2018) 'The CeNGEN Project: The Complete Gene Expression Map of an Entire Nervous System', *Neuron*. Cell Press, pp. 430–433. doi: 10.1016/j.neuron.2018.07.042.
Harbaugh, W. T., Krause, K. and Berry, T. R. (2001) 'GARP for Kids', *The American Economic Review*, 91(5), pp. 1539–1545.
Hendricks, M. *et al.* (2012) 'Compartmentalized calcium dynamics in a C. elegans interneuron encode head movement', *Nature*. Nature Publishing Group, 487, pp. 99–103. doi: 10.1038/nature11081.
Heufer, J. (2009) *Essays on revealed preference: contributions to the theory of consumer's behavior*. Available at: https://core.ac.uk/download/pdf/46909503.pdf.
Hobert, O. (2021) *Neurotransmitter map*. Available at: https://www.hobertlab.org/neurotransmitter-map/.
Hoenderop, J. G. J. *et al.* (1999) 'The epithelial calcium channel, ECaC, is activated by hyperpolarization and regulated by cytosolic calcium', *Biochemical and Biophysical Research Communications*, 261(2), pp. 488–492. doi: 10.1006/bbrc.1999.1059.
Houthakker, H. S. (1950) 'Revealed preference theory a tthe utility function', *Economica*, 17, pp. 159–174.
Huguenard, J. R. and McCormick, D. A. (2007) 'Thalamic synchrony and dynamic regulation of global forebrain oscillations', *Trends in Neurosciences*, 30(7), pp. 350–356. doi: 10.1016/j.tins.2007.05.007.
Hukema, R. K., Rademakers, S. and Jansen, G. (2008) 'Gustatory plasticity in C. elegans involves integration of negative cues and NaCl taste mediated by serotonin, dopamine, and glutamate', *Learning and Memory*, 15(11), pp. 829–836. doi: 10.1101/lm.994408.
Iino, Y. and Yoshida, K. (2009) 'Parallel Use of Two Behavioral Mechanisms for Chemotaxis in Caenorhabditis elegans', *Journal of Neuroscience*, 29(17), pp. 5370–5380. doi: 10.1523/JNEUROSCI.3633-08.2009.
Iwanir, S. *et al.* (2019) 'Irrational behavior in C. elegans arises from asymmetric modulatory effects within single sensory neurons', *Nature Communications*. Springer US, 10(1). doi: 10.1038/s41467-019-11163-3.
Jarrell, T. A. *et al.* (2012) 'The connectome of a decision-making neural network.', *Science (New York, N.Y.)*. American Association for the Advancement of Science, 337(6093), pp. 437–44. doi: 10.1126/science.1221762.
Jevons, W. . (1871) *The Theory of Political Economy*. London.: Macmillan and Co.
Kacelnik, A. (2006) 'Minimal rationality', in Hurley, S. L. and Nudds, M. (eds) *Rational Animals?* Oxford: Oxford University Press, pp. 87–106.
Kagel, J. *et al.* (1975) 'Experimental studies of consumer demand behavior using laboratory animals', *Economic Inquiry*, 13(1), pp. 22–38.
Kagel, J. H. *et al.* (1981) 'Demand curves for animal consumers', *Quarterly Journal of Economics*, 96(1), pp. 1–15.
Kagel, J. H., Battalio, R. C. and Green, L. (1995) *Economic Choice Theory*. Cambridge: Cambridge University Press.
Kalenscher, T., Wingerden, M. Van and Hayden, B. (2011) 'Why we should use animals to study economic decision making – a perspective', *Frontiers in Neuroscience*, 5(June), pp. 1–11. doi:

10.3389/fnins.2011.00082.
Kato, S. *et al.* (2013) 'Article Temporal Responses of C . elegans Chemosensory Neurons Are Preserved in Behavioral Dynamics', *Neuron*. Elsevier Inc., 81(3), pp. 616–628. doi: 10.1016/j.neuron.2013.11.020.
Kato, S. *et al.* (2015) 'Global Brain Dynamics Embed the Motor Command Sequence of Caenorhabditis elegans', *Cell*, 163(3). doi: 10.1016/j.cell.2015.09.034.
Keane, J. and Avery, L. (2003) 'Mechanosensory Inputs Influence Caenorhabditis elegans Pharyngeal Activity via Ivermectin Sensitivity Genes', *Genetics*, 164(May), pp. 153–162.
Kocabas, A. *et al.* (2012) 'elegans to evoke chemotactic behaviour', *Nature*. Nature Publishing Group, 490(7419), pp. 273–277. doi: 10.1038/nature11431.
Koch, A. L. (1970) 'Turbidity measure of bacterial cultures in some available commercial instruments', *Analytical Biochemistry*, 1, pp. 252–259.
Koga, M. and Ohshima, Y. (2004) 'The C . elegans ceh-36 Gene Encodes a Putative Homemodomain Transcription Factor Involved in Chemosensory Functions of ASE and AWC Neurons', *Journal of Molecular Biology*, 336, pp. 579–587. doi: 10.1016/j.jmb.2003.12.037.
Kopp-Scheinpflug, C., Sinclair, J. L. and Linden, J. F. (2018) 'When Sound Stops: Offset Responses in the Auditory System', *Trends in Neurosciences*, 41(10), pp. 712–728. doi: 10.1016/j.tins.2018.08.009.
Lanjuin, A. *et al.* (2003) 'Otx / otd Homeobox Genes Specify Distinct Sensory Neuron Identities in C . elegans', *Developmental Cell*, 5, pp. 621–633.
Latty, T. and Beekman, M. (2011) 'Irrational decision-making in an amoeboid organism : transitivity and context-dependent preferences', *Proceeding of the Royal Society B*, 278(August 2010), pp. 307–312. doi: 10.1098/rspb.2010.1045.
Lazzaro, S. C. *et al.* (2016) 'The impact of menstrual cycle phase on economic choice and rationality', *PLoS ONE*. Public Library of Science, 11(1). doi: 10.1371/journal.pone.0144080.
Lee, J., Jee, C. and McIntire, S. L. (2009) 'Ethanol preference in C. elegans', *Genes, Brain and Behavior*, 8(6), pp. 578–585. doi: 10.1111/j.1601-183X.2009.00513.x.
Lee, K. S. *et al.* (2017) 'Serotonin-dependent kinetics of feeding bursts underlie a graded response to food availability in C. elegans', *Nature Communications*. Nature Publishing Group, 8, pp. 1–11. doi: 10.1038/ncomms14221.
Lints, R. and Emmons, S. W. (1999) 'Patterning of dopaminergic neurotransmitter identity among Caenorhabditis elegans ray sensory neurons by a TGF β family signaling pathway and a Hox gene', *Development*, 5831, pp. 5819–5831.
Lockery, S. R. *et al.* (2012) 'A microfluidic device for whole-animal drug screening using electrophysiological measures in the nematode C. elegans', *Lab on a Chip*, 12(12). doi: 10.1039/c2lc00001f.
Mazur, J. E. and Coe, D. (1987) 'Test of transitivity in choices between fixed and variable reinforcer delays', *Journal of the Experimental Analysis of Behavior*, 47, pp. 287–297.
McCormick, K. E. *et al.* (2011) 'Microfluidic devices for analysis of spatial orientation behaviors in semi-restrained Caenorhabditis elegans', *PLoS ONE*, 6(10). doi: 10.1371/journal.pone.0025710.
Milward, K. *et al.* (2011) 'Neuronal and molecular substrates for optimal foraging in Caenorhabditis elegans'. doi: 10.1073/pnas.1106134109/-/DCSupplemental.www.pnas.org/cgi/doi/10.1073/pnas.1106134109.
Musselman, H. N. *et al.* (2012) 'Chemosensory cue conditioning with stimulants in a Caenorhabditis elegans animal model of addiction', *Behavioral Neuroscience*, 126(3), pp. 445–456. doi: 10.1037/a0028303.
Nehrke, K. *et al.* (2000) 'Model Organisms: New Insights Into Ion Channel and Transporter Function. Caenorhabditis elegans ClC-type chloride channels: novel variants and functional expression', *American Journal of Cell Physiology*, 279, pp. C2052–C2066. doi: 10.1007/978-3-030-53953-5_10.
Nguyen, J. P. *et al.* (2016) 'Whole-brain calcium imaging with cellular resolution in freely behaving Caenorhabditis elegans', *Proceedings of the National Academy of Sciences of the United States of America*, 113(8), pp. E1074–E1081. doi: 10.1073/pnas.1507110112.
Nickell, W. T. *et al.* (2002) 'Single ionic channels of two Caenorhabditis elegans chemosensory neurons in native membrane', *Journal of Membrane Biology*, 189(1), pp. 55–66. doi: 10.1007/s00232-002-1004-x.
Nilius, B. *et al.* (2000) 'Whole-cell and single channel monovalent cation currents through the novel rabbit epithelial Ca2+ channel ECaC', *Journal of Physiology*, 527(2), pp. 239–248. doi: 10.1111/j.1469-7793.2000.00239.x.
Padoa-schioppa, C. and Assad, J. A. (2006) 'Neurons in the orbitofrontal cortex encode economic value',

Nature, 441(May), pp. 223–226. doi: 10.1038/nature04676.
Pastor-Bernier, A., Stasiak, A. and Schultz, W. (2019) 'Orbitofrontal signals for two-component choice options comply with indifference curves of Revealed Preference Theory', *Nature Communications*, 10(1). doi: 10.1038/s41467-019-12792-4.
Pearson, J. M., Watson, K. K. and Platt, M. L. (2014) 'Decision Making : The Neuroethological Turn', *Neuron*, 82(June), pp. 950–965.
Press, W. H. *et al.* (2007) *Numerical Recipes*. 3rd edn. Cambridge University Press.
Raible, F. and Arendt, D. (2004) 'Metazoan Evolution: Some Animals Are More Equal than Others', *Current Biology*, 14(3), pp. R106–R108. doi: 10.1016/j.cub.2004.01.015.
Raizen, D. M. and Avery, L. (1994) 'Electrical Activity and Behavior in the Pharynx of Caenorhabditis elegans', *Neuron*, 12, pp. 483–495.
Roberts, A., Li, W. C. and Soffe, S. R. (2008) 'Roles for inhibition: Studies on networks controlling swimming in young frog tadpoles', *Journal of Comparative Physiology A: Neuroethology, Sensory, Neural, and Behavioral Physiology*, 194(2), pp. 185–193. doi: 10.1007/s00359-007-0273-3.
Rose, H. (1958) 'Consistency of Preference : The Two-Commodity Case', *The Review of Economic Studies*, 25(2), pp. 124–125.
Saeki, S., Yamamoto, M. and Iino, Y. (2001) 'Plasticity of chemotaxis revealed by paired presentation of a chemoattractant and starvation in the nematode Caenorhabditis elegans', *Journal of Experimental Biology*, 204(10), pp. 1757–1764.
Samuel, B. S. *et al.* (2016) 'Caenorhabditis elegans responses to bacteria from its natural habitats', *Proceedings of the National Academy of Sciences of the United States of America*, pp. E3941–E3949. doi: 10.1073/pnas.1607183113.
Samuelson, P. A. (1938) 'A note on the pure theory of consumer's behaviour', *Economica*, 51(17), pp. 61–71.
Sawin, E. R., Ranganathan, R. and Horvitz, H. R. (2000) 'C. elegans locomotory rate is modulated by the environment through a dopaminergic pathway and by experience through a serotonergic pathway', *Neuron*. doi: 10.1016/S0896-6273(00)81199-X.
Scholz, M. *et al.* (2016) 'A scalable method for automatically measuring pharyngeal pumping in C . elegans', *Journal of Neuroscience Methods*. Elsevier B.V., 274, pp. 172–178. doi: 10.1016/j.jneumeth.2016.07.016.
Schuck-Paim, C. and Kacelnik, A. (2002) 'Rationality in risk-sensitive foraging choices by starlings', *Animal Behaviour*, 64, pp. 869–879. doi: 10.1006/anbe.2002.2003.
Senior, N. (1836) *An Outline of the Science of Political Economy*. London: Encyclopaedia Metropolitana.
Shafir, S. (1994) 'Intransitivity of preferences in honey bees: support of "comparative" evaluation of foraging options', *Animal Behaviour*, 48, pp. 55–67.
Shinkai, Y., Yamamoto, Y., Fujiwara, M., Tabata, T., Murayama, T., Hirotsu, T., Ikeda, Daisuke D., *et al.* (2011) 'Behavioral choice between conflicting alternatives is regulated by a receptor guanylyl cyclase, GCY-28, and a receptor tyrosine kinase, SCD-2, in AIA interneurons of Caenorhabditis elegans', *Journal of Neuroscience*, 31(8), pp. 3007–3015. doi: 10.1523/JNEUROSCI.4691-10.2011.
Shinkai, Y., Yamamoto, Y., Fujiwara, M., Tabata, T., Murayama, T., Hirotsu, T., Ikeda, Daisuke D, *et al.* (2011) 'Cellular/Molecular Behavioral Choice between Conflicting Alternatives Is Regulated by a Receptor Guanylyl Cyclase, GCY-28, and a Receptor Tyrosine Kinase, SCD-2, in AIA Interneurons of Caenorhabditis elegans'. doi: 10.1523/JNEUROSCI.4691-10.2011.
Shtonda, B. B. and Avery, L. (2006) 'Dietary choice behavior in Caenorhabditis elegans', *Journal of Experimental Biology*. doi: 10.1242/jeb.01955.
Simon, H. A. (1957) *Models of Man*. New York: Wiley.
Song, B.-M. *et al.* (2013) 'Recognition of familiar food activates feeding via an endocrine serotonin signal in Caenorhabditis elegans', *eLife*, 2013(2). doi: 10.7554/eLife.00329.
Stevenson, K. *et al.* (2016) 'General calibration of microbial growth in microplate readers', *Scientific Reports, 6*, 6, p. 38828.
Sumpter, C. E., Temple, W. and Foster, T. . (1999) 'The transitivity of choices between different response requirements', *Journal of the Experimental Analysis of Behavior*, 72(2), pp. 235–249.
Tan, M. *et al.* (1999) 'Pseudomonas aeruginosa killing of Caenorhabditis elegans used to identify P. aeruginosa virulence factors', 96, pp. 2408–2413. Available at: www.pnas.org.
Tanimoto, Y. *et al.* (2016) 'In actio optophysiological analyses reveal functional diversification of dopaminergic neurons in the nematode C. elegans', *Scientific Reports*. doi: 10.1038/srep26297.

Torayama, I., Ishihara, T. and Katsura, I. (2007) 'Caenorhabditis elegans Integrates the Signals of Butanone and Food to Enhance Chemotaxis to Butanone', 27(4), pp. 741–750. doi: 10.1523/JNEUROSCI.4312-06.2007.

Varian, H. R. (1982) 'The NonparametricApproach to Demand Analysis', *Econometrica*, 50(4), pp. 945–973.

Varian, H. R. (1992) *Microeconomic Analsysis*. 3rd edn. W. W. Norton & Company.

Varian, H. R. (1995) 'Efficiency in production and consumption'.

Venkatachalam, V. *et al.* (2016) 'Pan-neuronal imaging in roaming Caenorhabditis elegans', *Proceedings of the National Academy of Sciences of the United States of America*, 113(8), pp. E1082–E1088. doi: 10.1073/pnas.1507109113.

Voglis, G. and Tavernarakis, N. (2008) 'A synaptic DEG/ENaC ion channel mediates learning in C. elegans by facilitating dopamine signalling', *EMBO Journal*, 27(24), pp. 3288–3299. doi: 10.1038/emboj.2008.252.

W K Bickel, L Green, R. E. V. (1995) 'Behavioral economics', *J Exp Anal Behav*, 64(3)(3), pp. 257–62.

Weeks, J. C. *et al.* (2018) 'Anthelmintic drug actions in resistant and susceptible C. elegans revealed by electrophysiological recordings in a multichannel microfluidic device', *International Journal for Parasitology: Drugs and Drug Resistance*, 8(3). doi: 10.1016/j.ijpddr.2018.10.003.

Wes, P. D. and Bargmann, C. I. (2001) 'C . elegans odour discrimination requires asymmetric diversity in olfactory neurons', *Nature*, 410(April), pp. 10–13.

White JG, Southgate E, Thomson JN, B. S. (1986) 'The structure of the nervous system of the nematode Caenorhabditis elegans', *Philosophical Transactions of the Royal Society of London. B, Biological Sciences*. The Royal Society, 314(1165), pp. 1–340. doi: 10.1098/rstb.1986.0056.

Worthy, S. E., Haynes, L., *et al.* (2018) 'Identification of attractive odorants released by preferred bacterial food found in the natural habitats of C . elegans', *PLoS ONE*, pp. 1–14. Available at: https://doi.org/10.1371/journal.pone.0201158.

Worthy, S. E., Rojas, G. L., *et al.* (2018) 'Identification of Odor Blend Used by Caenorhabditis elegans for Pathogen Recognition', *Chemical Senses*, 43(January), pp. 169–180. doi: 10.1093/chemse/bjy001.

Xia, Y. *et al.* (2008) 'Complex Optical Surfaces Formed by Replica Molding Against Elastomeric Masters Published by : American Association for the Advancement of Science Stable URL : http://www.jstor.org/stable/2889746', 273(5273), pp. 347–349.

Xia, Y. and Whitesides, G. M. (1998) 'Soft lithography', *Angewandte Chemie - International Edition*, 37(5), pp. 550–575. doi: 10.1002/(sici)1521-3773(19980316)37:5<550::aid-anie550>3.3.co;2-7.

Yapici, N., Zimmer, M. and Domingos, A. I. (2014) 'Cellular and molecular basis of decision-making', *EMBO reports*. EMBO, 15(10), pp. 1023–1035. doi: 10.15252/embr.201438993.

Zaslaver, A. *et al.* (2015) 'Hierarchical sparse coding in the sensory system of Caenorhabditis elegans', *Proceedings of the National Academy of Sciences of the United States of America*, 112(4), pp. 1185–1189. doi: 10.1073/pnas.1423656112.

Zhang, Y., Lu, H. and Bargmann, C. I. (2005) 'Pathogenic bacteria induce aversive olfactory learning in Caenorhabditis elegans', 438(November), pp. 179–184. doi: 10.1038/nature04216.

SUPPLEMENTARY INFORMATION

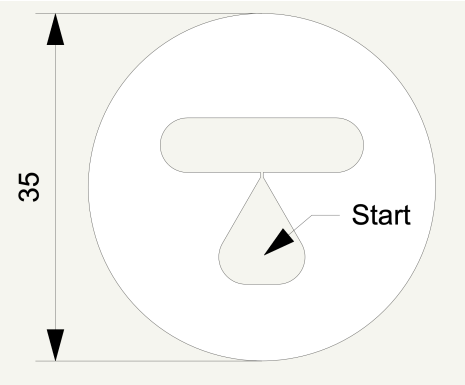

Supplemental Figure 1: T-maze

The teardrop shapped feature acts as worm diode. Worms leave the teardrop more easily than they re-enter it, thus helping to ensure the do not congregate at the starting point. The mask's ability to confine worms in the test area is improved by floating the maze on the surface of the agarose medium while it is still liquid (M. Brooks, pers. comm.). Dimensions are in mm.

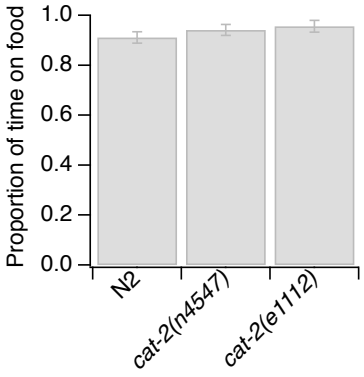

Supplemental Figure 2: Loss of dopamine signaling does not reduce proportion of time on food

Mutations in the gene *cat-2* do not significantly later the ability of worms to find and remain in food patches. Statistics (*t*-tests): N2 vs. *cat-2(n4547)*, $t(38) = -0.95$, $P = 0.35$; N2 vs *cat-2(e1112)*, $t(40) = -1.38$, $P = 0.18$.

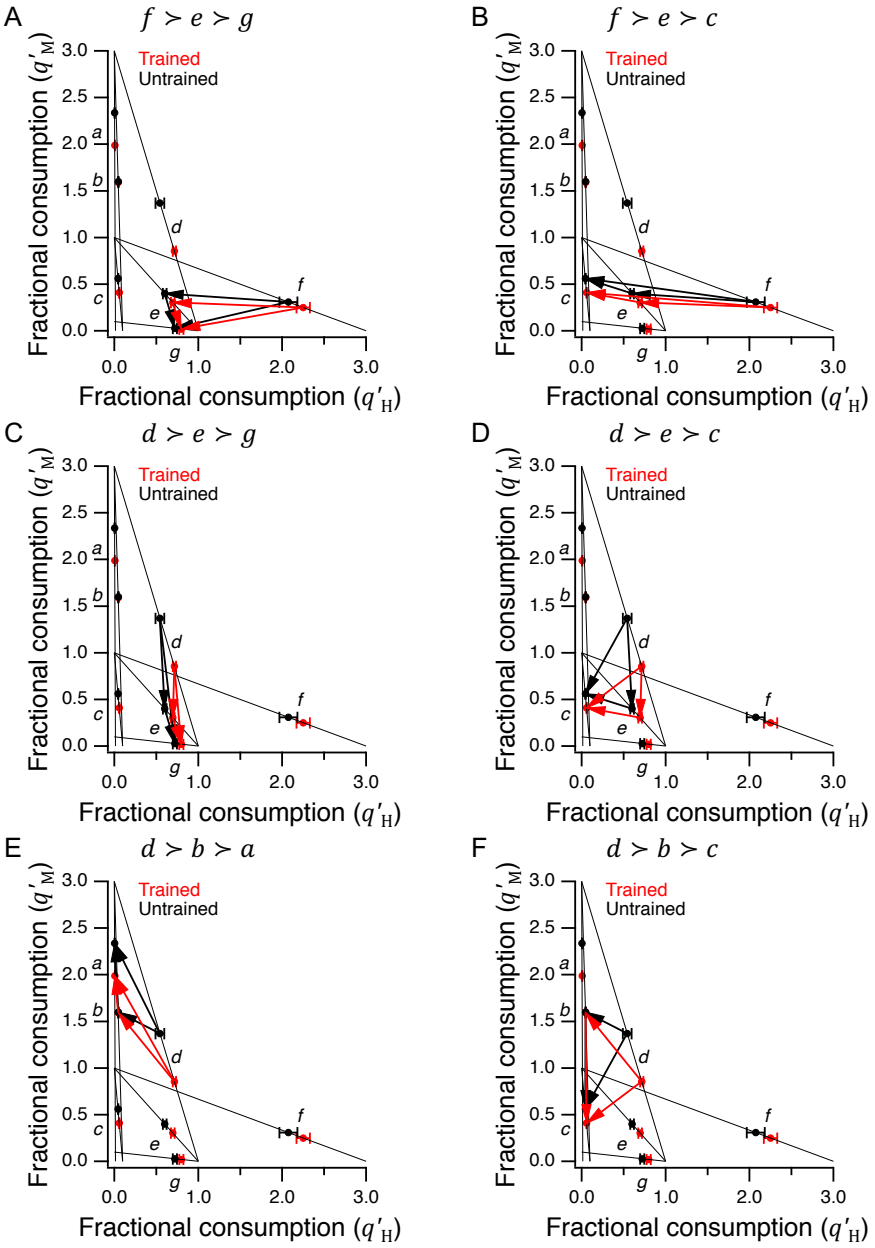

Supplemental Figure 3. Indirectly revealed preferences inherent in the choices shown in Fig. 5C

A-F. Italic lower case letters refer to the preferred option in each choice set, consistent with the labels in Fig. 5B,C. Arrows show pairwise preferences implied by the data set, such that $i \rightarrow j$ means $i \succ j$. There are no transitivity violations in that, for each triplet $i \succ j \succ k$, the arrow between the first and third option points in the direction $i \rightarrow k$, rather than $k \rightarrow i$.

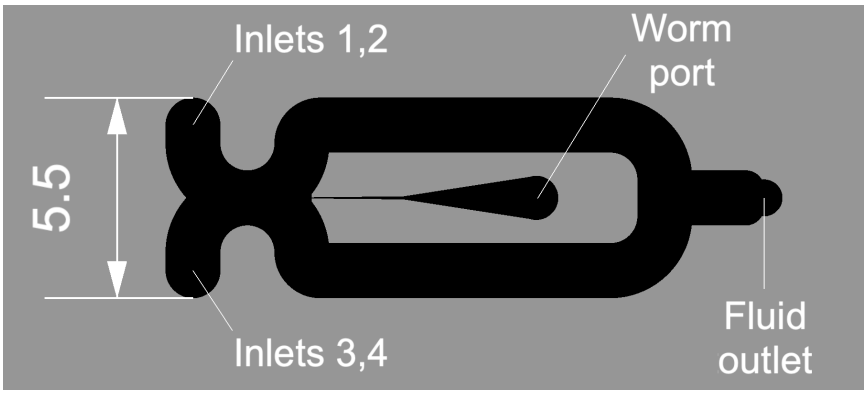

Supplemental Figure 4: Imaging chip

Fluidic features are shown in black. Dimensions are in mm.

Row	Figure	Test	Comparison	Statistic		*DF* 1	*DF* 2	*P*
1	2B*	Two-factor ANOVA, repeated measures, posthoc t-tests	N2, Trained vs. Untrained, post-hoc *t* -tests	*t*	2.50	7	–	**2.96E-02**
2	2B	*t* -test	N2, Untrained, 60 min mean *I* > 0	*t*	10.21	7	–	**1.86E-05**
3	2B	*t* -test	*ceh-36* , Untrained, 60 min mean *I* > 0	*t*	3.58	7	–	**9.00E-03**
4	2B	Two-factor ANOVA, repeated measures, main effect	Trained *ceh-36* vs. N2 Untrained	*F*	0.11	1	14	2.50E-01
5	2B	Two-factor ANOVA, repeated measures, main effect	Unrained *ceh-36* vs. N2 Untrained	*F*	2.50	1	14	1.74E-01
6	2B	Two-factor ANOVA, repeated measures, main effect	*ceh-36,* Trained vs. Untrained	*F*	0.66	1	14	5.70E-01
7	2C	Two-factor ANOVA, repeated measures, main effect	Azide-, Trained vs. Untrained	*F*	11.28	1	21	**2.98E-03**
8	2C	*t* -test	Azide+, Trained, 60 min mean *I* > 0	*t*	6.35	10	–	**8.36E-05**
9	2C	*t* -test	Azide+, Untrained, 60 min mean *I* > 0	*t*	3.09	10	–	**1.15E-02**
10	2C	Two-factor ANOVA, repeated measures, main effect	Azide+, Trained vs. Untrained	*F*	10.32	1	20	**4.37E-03**
11	2C	Two-factor ANOVA, repeated measures, main effect	Trained, Azide+ vs. Azide–	*F*	11.17	1	19	**3.43E-03**
12	2C	Two-factor ANOVA, repeated measures, main effect	Untrained, Azide+ vs. Azide–	*F*	38.28	1	22	**3.16E-06**
13	2D	Two-factor ANOVA, repeated measures, main effect	Untrained, N2 vs. *cat-2*	*F*	23.25	1	21	**9.14E-05**
14	2D	Two-factor ANOVA, repeated measures, main effect	Trained, N2 vs. *cat-2*	*F*	52.50	1	18	**9.74E-07**
15	2D	Two-factor ANOVA, repeated measures, main effect	*cat-2* , Trained vs. Untrained	*F*	0.90	1	18	6.43E-01
16	4A	Two-factor ANOVA, main effect	Familiar vs. unfamiliar	*F*	10.46	1	27	2.1E-03
17	4A	*t* -test	Unfamiliar, grown in H vs. grown in M	*t*	1.77	17	–	9.4E-02
18	4B	*t* -test	Trained, *f*_ H > 0.5	*t*	8.60	18	–	8.6E-08
19	4B	*t* -test	Trained, *f*_ H > 0.5	*t*	4.35	27	–	1.7E-04
20	4B*	*t* -test	Trained vs. Untrained	*t*	3.06	45	–	**3.75E-03**
21	4E	Two-factor ANOVA, main effect	Peak Frequency vs. Optical Density	*F*	31.58	3	108	***P* < .001**
22	4F	Two-factor ANOVA, main effect	Time to Half-max Pumping Rate vs. Optical Density	*F*	3.10	3	106	**3.00E-02**
23	5B	Two-factor ANOVA, main effect	Effect of price ratio	*F*	3.97	6	191	1.0E-03
24	5B	Two-factor ANOVA, main effect	Trained vs. Untrained	*F*	39.30	18	191	1.0E-03
25	5B	*t* -test	Trained, point *a* , mean *f*_ H < 0.5	*t*	6.22	8	–	**2.52E-04**
26	5B	*t* -test	Untrained, point *a* , mean *f*_ H < 0.5	*t*	8.29	11	–	**4.66E-06**
27	6A	Regression with replication slope test	Fig. 5B, points *abd* , Trained slope ≠ 0	*F*	118.79	1	47	**1.85E-14**
28	6A	Regression with replication slope test	Fig. 5B, points *abd* , Untrained slope ≠ 0	*F*	28.52	1	39	**4.26E-06**
29	6A	Regression with replication slope test	Fig. 5B, points *cef* , Trained slope ≠ 0	*F*	20.29	1	46	**4.54E-05**
30	6A	Regression with replication slope test	Fig. 5B, points *cef* , Untrained slope ≠ 0	*F*	26.56	1	49	**4.55E-06**
31	6A	Regression with replication slope test	Fig. 5B, points *deg* , Trained slope ≠ 0	*F*	2.34	1	51	1.32E-01
32	6A	Regression with replication slope test	Fig. 5B, points *deg* , Untrained slope ≠ 0	*F*	7.82	1	45	**7.56E-03**
33	7A	Regression	Frequency ratio vs. *f*_ H	*t*	-6.64	141	–	6.53E-10
34	7B	Regression	Dwell time ratio vs. *f*_ H	*t*	39.60	202	–	6.95E-97
35	7C	Regression	Dwell time ratio vs. mean head angle	*t*	35.96	202	–	**2.62E-89**
36	7D	t-test	*ceh-36* Untrained, *f*_ H > 0.5	*t*	4.20	10	–	**1.84E-03**
37	7D*	Two-factor ANOVA	Treatment × Strain interaction	*F*	5.03	1	62	**2.85E-02**
38	7D	*t* -test	*ceh-36* , Trained vs. Untrained	*t*	-0.58	16	–	5.68E-01
39	8B	Two-factor ANOVA, main effect	Fig. 8B, mean integrated *dF* /*F* , H vs. M food	*F*	3.56	1	23	7.20E-02
40	8D	Two-factor ANOVA, main effect	Fig. 8D, mean integrated *dF* /*F* , H vs. M food	*F*	18.42	1	25	**2.00E-04**
41	8C*	*t* -test	Peak response, Untrained, H vs. M food	*t*	2.98	12	–	**1.30E-02**
42	8C×	*t* -test	Peak response, Trained, H vs. M food	*t*	3.18	13	–	7.30E-03
43	8B	Two-factor ANOVA, main effect	Trained vs. Untrained	*F*	0.00	1	23	9.90E-01
44	8D	Two-factor ANOVA, main effect	Trained vs. Untrained	*F*	7.52	1	25	**1.10E-02**
45	8D*	*t* -test	H food, Trained vs. Untrained	*t*	2.86	12	–	**1.44E-02**
46	8D	*t* -test	M food, Trained vs. Untrained	*t*	-0.80	13	–	4.39E-01
47	9A*	*t* -test	H → M, peak response, Trained vs. Untrained	*t*	2.21	97	–	**3.00E-02**
48	9A	*t* -test	M → H, max response, Trained vs. Untrained	*t*	0.60	100	–	5.50E-01
49	9C	*t* -test	Trained, point *e* vs. Untrained, point *d*	*t*	2.14	25	–	4.23E-02

Supplemental Table 1. Statistics

P values associated with significant results are shown in bold font.

1541

	Trained	Untrained
Offer value H	$w_T \cdot d_H$	$w_U \cdot d_H$
Log offer value H	$\log(w_T \cdot d_H)$	$\log(w_U \cdot d_H)$
Offer value M	d_M	d_M
Log offer value M	$\log(d_M)$	$\log(d_M)$
Offer value	$w_T \cdot d_H + d_M$	$w_U \cdot d_H + d_M$
Log offer value	$\log(w_T \cdot d_H + d_M)$	$\log(w_U \cdot d_H + d_M)$
Δ Offer value	$-w_T \cdot d_H + d_M$	$-w_U \cdot d_H + d_M$
Δ Log offer value	$-\log(w_T \cdot d_H) + \log(d_M)$	$-\log(w_U \cdot d_H) + \log(d_M)$
Chosen value	$w_T \cdot f_H \cdot d_H + (1 - f_H) \cdot d_M$	$w_U \cdot f_H \cdot d_H + (1 - f_H) \cdot d_M$
Log chosen value	$\log(w_T \cdot f_H \cdot d_H + (1 - f_H) \cdot d_M)$	$\log(w_U \cdot f_H \cdot d_H + (1 - f_H) \cdot d_M)$
Δ Chosen value	$-w_T \cdot f_H \cdot d_H + (1 - f_H) \cdot d_M$	$-w_U \cdot f_H \cdot d_H + (1 - f_H) \cdot d_M$
Δ Log chosen value	$-\log(w_T \cdot f_H \cdot d_H) + \log((1 - f_H) \cdot d_M)$	$-\log(w_U \cdot f_H \cdot d_H) + \log((1 - f_H) \cdot d_M)$
Offer utility H	$U_T(d_H, 0)$	$U_U(d_H, 0)$
Offer utility M	$U_T(0, d_M)$	$U_U(0, d_M)$
Offer utility	$U_T(d_H, d_M)$	$U_U(d_H, d_M)$
Δ Offer utility	$-U_T(d_H, 0) + U_T(0, d_M)$	$-U_U(d_H, 0) + U_U(0, d_M)$
Chosen utility	$U_T(f_H \cdot d_H, (1 - f_H) \cdot d_M)$	$U_U(f_H \cdot d_H, (1 - f_H) \cdot d_M)$
Δ Chosen utility	$-U_T(f_H \cdot d_H, 0) + U_T(0, (1 - f_H) \cdot d_M)$	$-U_U(f_H \cdot d_H, 0) + U_U(0, (1 - f_H) \cdot d_M)$

Supplemental Table 2: Linear correlation equations

These equations show how the economic variables in the left column were computed based on food type and density in trained and untrained animals. The quantities w_T and w_U are defined in equation 13 in the main text. The quantities U_T and U_U are, respectively, utility in trained and untrained animals computed according to the CES function as fitted to the data in Fig. 6C,D.

	Trained					Untrained				
	r^2	*F*	DF1	DF2	*P*	r^2	*F*	DF1	DF2	*P*
Offer value H	0.004	0.021	1	5	0.891	0.017	0.086	1	5	0.781
Log offer value H	0.255	1.710	1	5	0.248	0.134	0.774	1	5	0.419
Offer value M	0.106	0.594	1	5	0.476	0.005	0.027	1	5	0.875
Log offer value M	0.017	0.087	1	5	0.780	0.010	0.049	1	5	0.834
Offer value	0.003	0.014	1	5	0.912	0.015	0.077	1	5	0.793
Log offer value	0.174	1.053	1	5	0.352	0.046	0.240	1	5	0.645
Δ Offer value	0.006	0.029	1	5	0.872	0.017	0.089	1	5	0.778
Δ Log offer value	0.174	1.053	1	5	0.352	0.046	0.240	1	5	0.645
Chosen value	0.001	0.003	1	5	0.959	0.000	0.002	1	5	0.968
Log chosen value	0.098	0.541	1	5	0.495	0.007	0.035	1	5	0.858
Δ Chosen value	0.004	0.019	1	5	0.896	0.013	0.068	1	5	0.805
Δ Log chosen value	0.199	1.241	1	5	0.316	0.059	0.314	1	5	0.600
Offer utility H	0.162	0.965	1	5	0.371	0.098	0.541	1	5	0.495
Offer utility M	0.035	0.183	1	5	0.687	0.003	0.016	1	5	0.903
Offer utility	0.139	0.804	1	5	0.411	0.147	0.865	1	5	0.395
Δ Offer utility	0.151	0.890	1	5	0.389	0.043	0.225	1	5	0.655
Chosen utility	0.125	0.715	1	5	0.436	0.130	0.749	1	5	0.426
Δ Chosen utility	0.105	0.586	1	5	0.478	0.130	0.749	1	5	0.426

Supplemental Table 3: Tests of linear correlations between AWC activation and economic variable it might hypothetically represent

Significance of correlations was tested using the *F* distribution. This table shows, for each economic variable tested, the correleation coefficient, value of the *F* statistic, its two degrees of freedom, and the corresponding *P* value. No significant correlations where found. Definitions of variable are proviced in Supplemental Table 2.

T-maze	https://www.dropbox.com/s/xxy5ttfqtnqlv56/T-maze-CAD.dwg?dl=0
Y-chip	https://www.dropbox.com/s/sw8df35mcy03ymz/Y-chip-CAD.dwg?dl=0
Imaging-chip	https://www.dropbox.com/s/1z7ne8crarzbk5f/Imaging-chip-CAD.dwg?dl=0

Supplementary Table 4: CAD Files

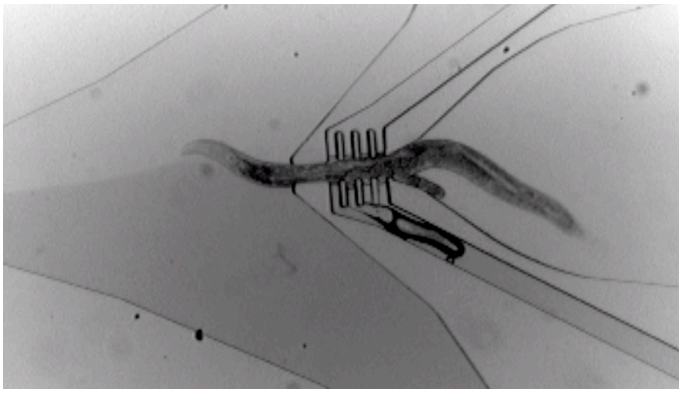

Supplemantary Video 1: Foraging behavior in the Y-chip

The worms held at its midsection by a vacuum activated clamp, leaving the head (left) and tail free to move. Bubbles orinating at the clamp are formed by air that has been pulled through the PDMS walls of the chip by the vacuum. The fluid streams contain M9 buffer, flowing to the left. Food dye was added to the lower stream to visualize the interface between streams. The worm preferrs the dye as it contains potassium sorbate, which acts as a chemoattractant.

https://www.dropbox.com/s/h307zd8g3nsv4cc/Y-chip-video.mov?dl=0